GENETICS

Dual mechanism of inflammation sensing by the hematopoietic progenitor genome

Vu L. Tran[1], Peng Liu[2], Koichi R. Katsumura[1], Alexandra A. Soukup[1], Audrey Kopp[1], Zamaan S. Ahmad[1], Ashley E. Mattina[1], Marjorie Brand[1], Kirby D. Johnson[1], Emery H. Bresnick[1]*

Genomes adapt dynamically to alterations in the signaling milieu, including inflammation that transiently or permanently disrupts genome function. Here, we elucidate how a progenitor cell genome senses and responds to inflammation when the developmental and transcriptional regulator GATA2 is limiting, which causes bone marrow failure in humans and mice and predisposes to leukemia in humans. GATA2^{low} murine progenitors are hypersensitive to inflammatory mediators. We discovered that the hematopoietic transcription factor PU.1 conferred transcriptional activation in GATA2^{low} progenitors in response to Interferon-γ and Toll-Like Receptor 1/2 agonists. In a locus-specific manner, inflammation reconfigured genome activity by promoting PU.1 recruitment to chromatin or tuning activity of PU.1-preoccupied chromatin. The recruitment mechanism disproportionately required IKKβ activity. Inflammation-activated genes were enriched in motifs for RUNX factors that cooperate with GATA factors. Contrasting with the GATA2-RUNX1 cooperativity paradigm, GATA2 suppressed and RUNX1 promoted PU.1 mechanisms to endow the progenitor genome with inflammation-sensing capacity.

INTRODUCTION

Inflammation is vital for healing, yet dysregulated and/or excessive inflammation is deleterious to cells (*1*). Inflammatory cytokines and chemokines activate cell-surface receptors, instigating genomic and non-genomic mechanisms that control cellular biology and physiology (*1*). Given the numerous inflammatory mediators and effectors that affect chromatin and transcription, and inflammation promoting bone marrow failure and leukemia (*2*–*5*), it is instructive to consider how genomes sense and respond to inflammation. Although inflammation activates common transcription factors, e.g., Nuclear Factor κB (NF-κB) and Activator Protein-1 (AP-1), there are many unanswered questions regarding how inflammation affects genome function.

We discovered that reducing the levels of GATA2, a hematopoietic transcription factor essential for hematopoietic stem and progenitor cell (HSPC) development, activates genes encoding diverse inflammatory components (*6*–*9*). Although GATA2 is not recognized as an inflammation-regulated transcription factor, oncogenic Ras/Mitogen-Activated Protein Kinase induces GATA2 phosphorylation, increasing its transcriptional regulatory activity (*10*, *11*). In GATA2-deficient murine fetal progenitors (GATA2^{low}), expression of genes encoding Interferon-γ (IFN-γ) receptor and Toll-Like Receptor 1/2 (TLR1/2) and TLR2/6 is up-regulated, and their agonists induce transcriptional responses considerably greater than in wild-type progenitors (*6*, *8*). Reexpressing GATA2 in GATA2^{low} progenitors reduces the elevated expression of inflammatory components (*6*–*8*). Pathogenic variants are defective in lowering the elevated inflammation-dependent transcriptional response (*7*, *9*, *12*). Human *GATA2* heterozygous genetic variation causes an immunodeficiency disorder termed GATA2 Deficiency Syndrome involving a bone marrow failure and acute myeloid leukemia (AML) predisposition (*13*, *14*). *Gata2* heterozygous mice and compound heterozygous mice with a human disease variant and enhancer-deleted allele, modeling epigenetic silencing of the normal allele, are relatively normal in the steady state, yet chemotherapy or inflammation induces bone marrow failure (*15*–*17*). As inflammation promotes bone marrow failure and leukemia (*18*, *19*), a leukemia predisposition variant combined with genome hypersensitivity to inflammation may have critical pathogenic implications.

Analogous to GATA2 deficiency, bone marrow granulocyte macrophage progenitors (GMPs) lacking the hematopoietic factor RUNX1 generate neutrophils with elevated IFN-α and TLR4 signaling (*20*, *21*). Germline RUNX1 deficiency creates Familial Platelet Disorder with a predisposition to myeloid malignancy (*22*, *23*). RUNX1 occupies loci encoding multiple components of these pathways, and RUNX1 loss increases accessibility of these loci (*21*). The E26 Transformation-Specific (ETS)-domain factor ETS Variant 6 (ETV6) functions as a repressor to control HSPC function during stress hematopoiesis (*24*). Germline *ETV6* variants create a predisposition for acute lymphoblastic leukemia and thrombocytopenia (*25*). An inhibitory *ETV6* germline variant (R355X) elevates inflammatory gene expression in bone marrow of a mouse model (*24*). HSPC functional defects can be associated with up-regulated inflammatory components and may render cells hypersensitive to inflammatory mediators.

In GATA2^{low} primary and ER-HOXB8–immortalized (hi-) murine fetal progenitors, GATA2 deficiency elevates activity of the ETS transcription factor PU.1 to induce a myeloid and B lineage gene expression program, including inflammatory genes (*7*). GATA2 and PU.1 can be antagonistic, and balancing their activities ensures normal hematopoiesis (*26*, *27*). Genetic ablation of a *Gata2* allele promotes AML instigated by another ETS factor ETS-Related Gene (ERG) in a transgenic mouse model, and GATA2 opposes ERG (*28*). Although multiple lines of evidence support GATA2-ETS antagonism, the importance of this mechanism for HSPC genome sensing of inflammation is unknown.

To understand how transcription factor levels establish genome sensing and responsiveness to inflammation, we leveraged a system in which deletion of a *Gata2* enhancer 77 kb upstream (−77) of the

[1]Wisconsin Blood Cancer Research Institute, Department of Cell and Regenerative Biology, Carbone Cancer Center, University of Wisconsin School of Medicine and Public Health, Madison, WI, USA. [2]Department of Biostatistics and Biomedical Informatics, Carbone Cancer Center, University of Wisconsin School of Medicine and Public Health, Madison, WI, USA.
*Corresponding author. Email: ehbresni@wisc.edu

promoter down-regulates GATA2 by ~75% in progenitors, including common myeloid progenitors (CMPs) and GMPs (*6*–*8*, *29*). Herein, we elucidated the mechanism underlying hypersensitivity of GATA2^{low} progenitors to inflammation by using GATA2^{low} progenitors that express ~50% less PU.1 and analyzing how these factors and IFN-γ–TLR1/2 signaling target the genome. The genome-sensing mechanism involved inflammation-induced GATA2 and PU.1 recruitment to chromatin at a gene cohort and constitutive GATA2 and PU.1 occupancy at another cohort. Contrasting with a GATA2-RUNX1 cooperativity paradigm, their opposing activities dictated PU.1-dependent genome responses to inflammation, and they differentially conferred responses to qualitatively distinct inflammatory signals.

RESULTS

TLR signaling contribution to GATA2-deficient hematopoietic progenitor levels and activities

GATA2 deficiency in primary and immortalized fetal myelo-erythroid progenitors up-regulates genes encoding IFN-γ and TLR signaling pathway components, conferring hypersensitivity to inflammation (*6*, *8*). Hypersensitivity is associated with reduced granulocytic progenitors (GPs) and increased monocytic progenitors (MPs) with retention of monocytic differentiation ex vivo (*6*, *29*, *30*). The transcription factor IFN Regulatory Factor 8 (IRF8) functions downstream of IFN-γ signaling to promote monocytic differentiation (*31*, *32*). Genetic ablation of *Irf8* in *Gata2* $-77^{-/-}$ embryos counteracted the disproportionately high monocytic differentiation (*30*). Because GATA2 deficiency elevates IFN-γ– and TLR-induced transcription (*8*), we asked whether attenuating the elevated TLR signaling of GATA2^{low} progenitors mimics *Irf8* ablation to normalize lineage output. As Myeloid Differentiation Primary Response 88 (MYD88) is an adaptor crucial for canonical permutations of TLR1/2 and TLR2/6 signaling (*33*, *34*), we ablated *Myd88* to attenuate TLR signaling in vivo. We generated $-77^{+/-}$;*Myd88*$^{-/-}$ mice and, with two mating schemes, generated $-77^{+/+}$, $-77^{-/-}$, *Myd88*$^{-/-}$, and $-77^{-/-}$;*Myd88*$^{-/-}$ embryonic day 14.5 (E14.5) embryos to analyze signaling and progenitors (Fig. 1A).

$-77^{-/-}$;*Myd88*$^{-/-}$ embryos were anemic with reduced liver size and cell numbers, resembling $-77^{-/-}$ embryos (Fig. 1, B and C). In $-77^{-/-}$ fetal livers, *Irf8*, *Tlr1*, *Tlr2*, and *Tlr6* expression was elevated as described (Fig. 1D) (*6*–*8*). *Myd88* loss in $-77^{-/-}$ embryos did not affect *Gata2* expression or up-regulated *Irf8*, *Tlr1*, *Tlr2*, and *Tlr6* expression. *Myd88* ablation abrogated elevated TLR1/2 agonist (Pam_3CSK_4)–induced activation (without or with IFN-γ) of TLR and IFN-γ target genes Tumor Necrosis Factor (*Tnf*) and C-X-C Motif Chemokine Ligand 10 (*Cxcl10*) in GATA2^{low} Lin$^-$ progenitors (Fig. 1E). Because *Myd88* ablation blocked TLR1/2-activated transcription in $-77^{-/-}$ progenitors, we asked whether this reversed the GP:MP imbalance. Using CD115 expression, Ly6C$^+$ GMPs were parsed into GP and MP populations (fig. S1, A and B) (*30*, *31*). Unlike IRF8 loss, MYD88 loss did not reverse the GP:MP imbalance (Fig. 1F).

Because $-77^{-/-}$ and *Myd88*$^{-/-}$ embryos had smaller livers, we tested whether MYD88 loss reduced total progenitor numbers. GATA2 deficiency increased CMP in fetal liver 1.8-fold ($P = 0.0081$). MYD88 loss decreased CMP 2.2-fold ($P = 0.024$) (Fig. 1G). CMP levels were comparable in $-77^{-/-}$;*Myd88*$^{-/-}$ and wild-type littermates. Relative to wild-type embryos, megakaryocytic-erythroid progenitors (MEPs) in $-77^{-/-}$ livers were 12-fold lower ($P < 0.0001$). MYD88 loss reduced MEPs 3.3-fold ($P < 0.0001$). MEPs were 37-fold ($P < 0.0001$) lower in $-77^{-/-}$;*Myd88*$^{-/-}$ versus wild-type. Thus, MYD88 contributes to establishment and/or maintenance of MEPs in GATA2^{low} fetal liver. MYD88 loss, with or without −77 ablation, reduced the GMP population relative to wild type (2.3-fold, $P = 0.0087$, and 1.8-fold, $P = 0.0031$, respectively). Ly6C$^-$ GMPs were unaffected by −77 deletion but decreased upon MYD88 loss (2.3-fold, $P = 0.012$). Among the Ly6C$^+$ GMPs, GP numbers decreased 2.8-fold ($P = 0.0002$) and 2.1-fold ($P = 0.0028$) upon GATA2 deficiency and MYD88 loss, respectively. GP levels decreased an additional 7.1-fold ($P < 0.0001$) in $-77^{-/-}$;*Myd88*$^{-/-}$ versus wild-type. Although MYD88 loss reduced MPs 2.9-fold ($P = 0.0121$), $-77^{-/-}$;*Myd88*$^{-/-}$ MPs were comparable to wild-type and slightly less than $-77^{-/-}$. These studies indicated that compromising TLR signaling reduced GPs and MPs without normalizing the imbalanced GP to MP ratio of GATA2^{low} fetal livers (Fig. 1H), differing from the ramifications of disrupting IFN-γ function via IRF8 loss.

To determine whether compromised TLR signaling affects $-77^{-/-}$ progenitor function, progenitor activity was quantified with sorted E14.5 fetal liver CMPs and GMPs in a colony-forming unit (CFU) assay. By comparison to $-77^{+/+}$ CMPs, $-77^{-/-}$ and *Myd88*$^{-/-}$ CMPs produced fewer (1.9-fold, $P = 0.0097$, and 2.0-fold, $P = 0.007$, respectively) CFU-G colonies (Fig. 2A). CFU-G generation from $-77^{-/-}$;*Myd88*$^{-/-}$ CMPs was even lower (5.2-fold, $P < 0.0001$) (Fig. 2A). These results were concordant with reduced GPs detected by flow cytometry (Fig. 1G). Thus, GATA2 and MYD88 collectively increased CMP-derived CFU-G. −77 deletion abrogated GMP-derived CFU-G, and MYD88 loss did not further affect CFU-G or elevated CFU-M (Fig. 2B). GATA2 deficiency abrogated CMP-derived CFU-GEMM, and MYD88 loss did not affect CFU-GEMM (Fig. 2A). Individual or dual ablation of *Gata2* −77 and *Myd88* did not affect CMP- or GMP-derived CFU-GM (Fig. 2). Analyses with the $-77^{-/-}$;*Myd88*$^{-/-}$ model, combined with our prior *Irf8*$^{-/-}$ analysis, revealed differential importance of distinct inflammatory mechanisms (IFN-γ versus TLR pathways) for the lineage output of GATA2^{low} fetal livers.

Distinct GATA2 and PU.1 activities confer inflammation-induced transcriptional responses

Although GATA2, IRF8, and MYD88 control critical aspects of myeloid progenitor development and/or function, our analyses described above revealed functional differences between IRF8 and MYD88, and mechanistic relationships are unresolved. GATA2 deficiency elevates activity of the hematopoietic transcription factor PU.1 to promote myeloid and B-lineage expression programs without affecting PU.1 levels (*7*). IRF8 and transcription factors activated by IFN-γ and TLR signaling, such as NF-κB, and AP-1, can co-occupy chromatin with PU.1 (*35*–*37*). Analysis of GATA2^{low} progenitor transcriptomes revealed that genes activated by MYD88-dependent inflammatory signaling harbor motifs for signal-dependent factors and lineage-determining factors, including ETS motifs bound by PU.1 (*8*). We hypothesized that PU.1 functions in inflammatory mechanisms involving GATA2, IRF8, and MYD88.

To establish whether PU.1 is essential, contributory, or not required for IFN-γ– and TLR1/2-mediated genomic responses, we used GATA2- and PU.1-deficient (hi-$77^{-/-}$;*Spi1*URE$^{-/-}$) fetal progenitors (Fig. 3A). Expression of *Spi1*, encoding PU.1, is controlled by a −14-kb enhancer [upstream regulatory element (URE)] (*38*, *39*). *Spi1* URE deletion reduced *Spi1* expression (Fig. 3B) 3.8-fold

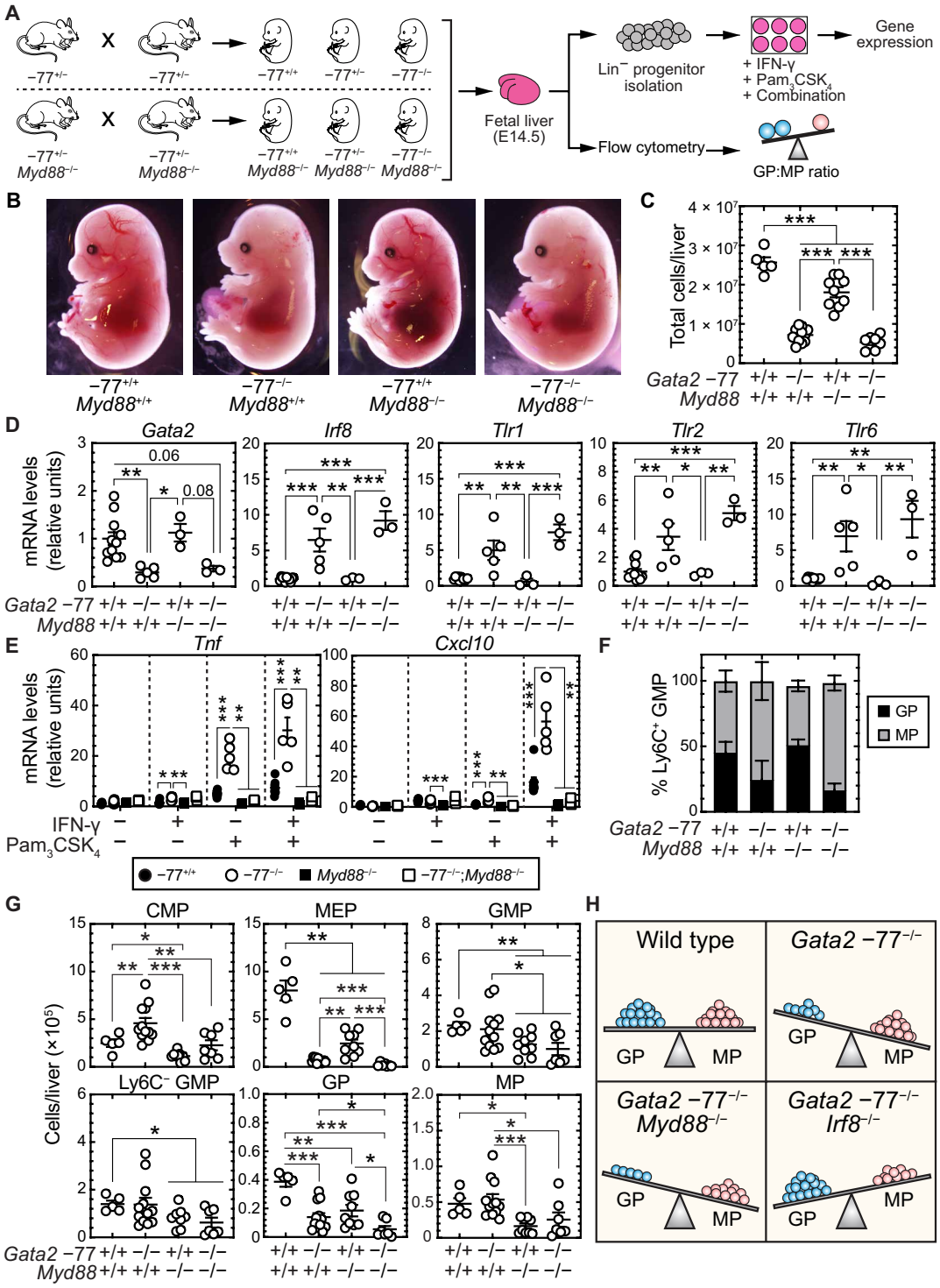

Fig. 1. *Myd88* ablation does not normalize the disproportionately high monocytic to granulocytic progenitor ratio of GATA2^{low} mouse embryos. (**A**) Strategy for attenuating TLR signaling. Embryonic day 14.5 (E14.5) fetal livers from two timed mating schemes (−77$^{+/−}$ and −77$^{+/−}$;*Myd88*$^{−/−}$) were harvested, and lineage-depleted progenitors were isolated and treated with IFN-γ (1 ng/ml), Pam_3CSK_4 (100 ng/ml), or both for 4 hours. In parallel, fetal livers were harvested for flow cytometry to quantify the cellular composition and GP versus MP ratios. (**B**) Representative E14.5 embryos obtained from the mating schemes in (A). (**C**) Total cellularity of E14.5 fetal livers. (**D**) The expression of select genes was quantitated using RT-qPCR. (**E**) The responsiveness of *Tnf* and *Cxcl10* to IFN-γ and Pam_3CSK_4 was quantitated using RT-qPCR. Statistics in (C) and (D) were one-way analysis of variance (ANOVA) with Tukey's multiple comparisons test and in (E) were multiple unpaired *t* tests. (**F**) Quantitation of MP and GP frequency within the Ly6C$^+$ GMP population in E13.5 to E14.5 fetal liver obtained from eight litters. (**G**) Quantitation of progenitor populations in E14.5 fetal livers obtained from seven litters. Error bars for all plots represent means ± SD. *$P < 0.05$; **$P < 0.01$; ***$P < 0.001$; Welch's unequal variance *t* tests. (**H**) Model depicting *Irf8*, but not *Myd88*, ablation reverses the GP:MP imbalance resulting from *Gata2* −77 enhancer deletion. Although the levels of GPs and MPs were reduced by *Myd88* ablation, the ratio was not altered.

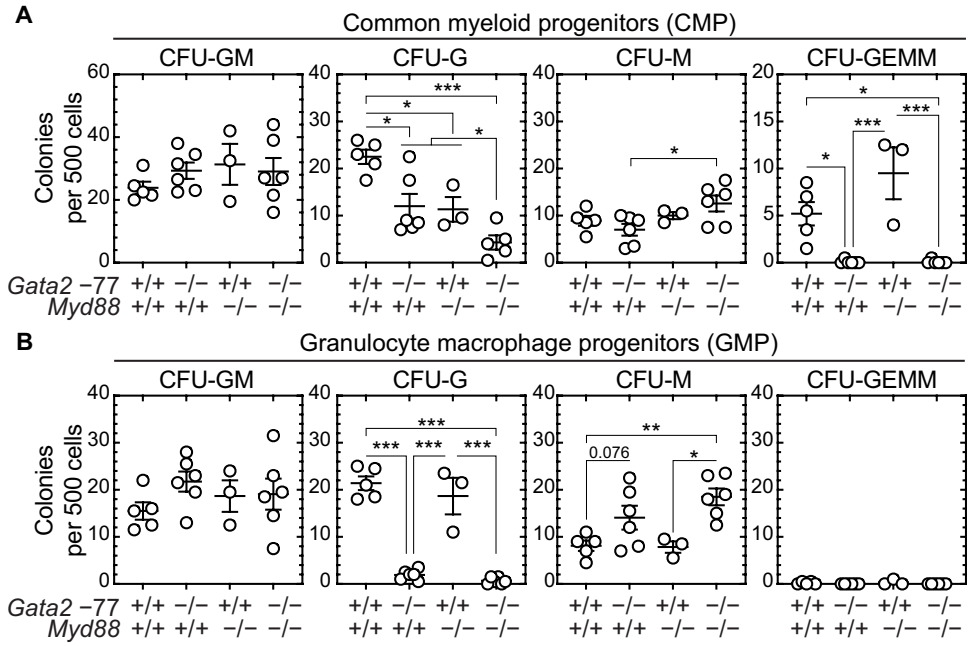

Fig. 2. TLR signaling promotes hematopoietic progenitor granulopoietic activity in GATA2^{low} mouse embryos. Quantitation of colonies from sorted CMP (**A**) and GMP (**B**) (five litters) plated in M3434 methylcellulose media at 500 cells per plate. Colonies were enumerated for erythroid, granulocyte, and monocyte content as CFU-GM, CFU-G, CFU-M, or CFU-GEMM. Error bars for all plots represent means ± SD. Statistics: Welch's unequal variance *t* tests. **P* < 0.05; ***P* < 0.01; ****P* < 0.001.

($P < 0.001$) and PU.1 (Fig. 3C) 2.1-fold ($P < 0.0001$). Although *Gata2* mRNA was unaffected, GATA2 protein increased 1.8-fold ($P = 0.0084$) in hi-77$^{-/-}$;*Spi1*URE$^{-/-}$ versus hi-77$^{-/-}$ cells. hi-77$^{-/-}$ and hi-77$^{-/-}$;*Spi1*URE$^{-/-}$ progenitors were treated with vehicle, IFN-γ, TLR1/2 agonist Pam_3CSK_4, or both agents for 4 hours, and RNA sequencing (RNA-seq) analysis was conducted (Fig. 3A). As an additional control, hi-77$^{+/+}$ were treated with or without both agents. Principal components analysis revealed reproducible RNA-seq data from four biological replicates (fig. S2A).

To determine the PU.1 contribution to TLR1/2-regulated transcription, we compared Pam_3CSK_4-induced differentially expressed genes (DEGs) between hi-77$^{-/-}$ and hi-77$^{-/-}$;*Spi1*URE$^{-/-}$ progenitors. Pam_3CSK_4 activated 33 genes in hi-77$^{-/-}$ cells, and lowering PU.1 ablated responses of 27 of these genes (Fig. 3D). Gene Ontology (GO) revealed that these PU.1-activated genes are linked to inflammatory response, cellular response to lipopolysaccharide (LPS), and negative regulation of Inhibitor of Nuclear Factor κB (IκB) kinase/NF-κB signaling (fig. S2B). Although six TLR-regulated genes retained regulation in hi-77$^{-/-}$;*Spi1*URE$^{-/-}$ progenitors, the magnitude of Pam_3CSK_4-induced expression was lower in hi-77$^{-/-}$;*Spi1*URE$^{-/-}$ versus hi-77$^{-/-}$ cells (Fig. 3D). PU.1 is, therefore, essential for TLR1/2-induced transcription in GATA2^{low} progenitors.

Contrasting with TLR responses, reducing PU.1 in GATA2^{low} progenitors did not alter responses of 115 IFN-γ–activated genes, 87% of which were induced to a similar magnitude in hi-77$^{-/-}$ and hi-77$^{-/-}$;*Spi1*URE$^{-/-}$ cells (Fig. 3E). Twenty-nine genes lost responsiveness to IFN-γ in hi-77$^{-/-}$;*Spi1*URE$^{-/-}$ versus hi-77$^{-/-}$ cells, reflecting their dependence upon PU.1 concentration (Fig. 3E). IFN-γ repressed a small number of genes in hi-77$^{-/-}$ and hi-77$^{-/-}$;*Spi1*URE$^{-/-}$ cells (fig. S2C). GO analysis revealed that the PU.1-activated genes are linked to negative regulation of biological processes, innate immune response, viral genome replication, and RNA polymerase II transcription (fig. S2D). IFN-γ signaling activated 38 genes in hi-77$^{-/-}$;*Spi1*URE$^{-/-}$ cells that were not activated in hi-77$^{-/-}$ cells (Fig. 3E). Lowering PU.1 impaired transcriptional responses of certain, but not all, IFN-γ–activated genes in GATA2^{low} progenitors.

Because lowering PU.1 in hi-77$^{-/-}$ cells decreased TLR1/2- and attenuated IFN-γ–mediated transcription, we hypothesized that hi-77$^{-/-}$;*Spi1*URE$^{-/-}$ progenitors might respond to IFN-γ and TLR1/2 agonist similarly to IFN-γ alone. Reducing PU.1 decreased responses of 69 genes and conferred responsiveness of 42 genes that were not activated in hi-77$^{-/-}$ cells (Fig. 3F). Although TLR signaling did not repress genes, the combined signaling repressed two-fold (in hi-77$^{-/-}$;*Spi1*URE$^{-/-}$) to four-fold (in hi-77$^{-/-}$) more genes versus IFN-γ signaling alone (fig. S2E). Reducing PU.1 did not alter the responsiveness of 148 genes to inflammation (Fig. 3F). Among these genes, 33 (22%) were induced to a greater extent, and 24 (16%) induced less in hi-77$^{-/-}$;*Spi1*URE$^{-/-}$ versus hi-77$^{-/-}$ progenitors (fig. S2F). To test whether altered TLR1/2 and IFN-γ responses reflect dysregulation of the respective receptors, we quantified receptor mRNA levels. Lowering PU.1 abrogated up-regulated *Tlr1* and *Tlr2* expression without affecting *Ifngr1* and *Ifngr2* (Fig. 3G). Thus, inflammation-activated genes in GATA2^{low} progenitors can be sensitive or insensitive to PU.1. Furthermore, the defective responses are associated with reduced *Tlr1* and *Tlr2* expression.

Our prior study revealed synergistic IFN-γ and TLR responses to induce cytokine/chemokine expression and production in GATA2^{low} progenitors (*8*), but the mechanisms were not elucidated. To determine whether PU.1 mediates synergistic responses in GATA2^{low} progenitors, we asked whether reducing PU.1 disrupts synergism. Among 217 IFN-γ– and Pam_3CSK_4-activated genes, 178 genes were regulated synergistically (Fig. 4A). GATA2 repressed the response of 79 of these genes. Parsing the genes based on PU.1-mediated

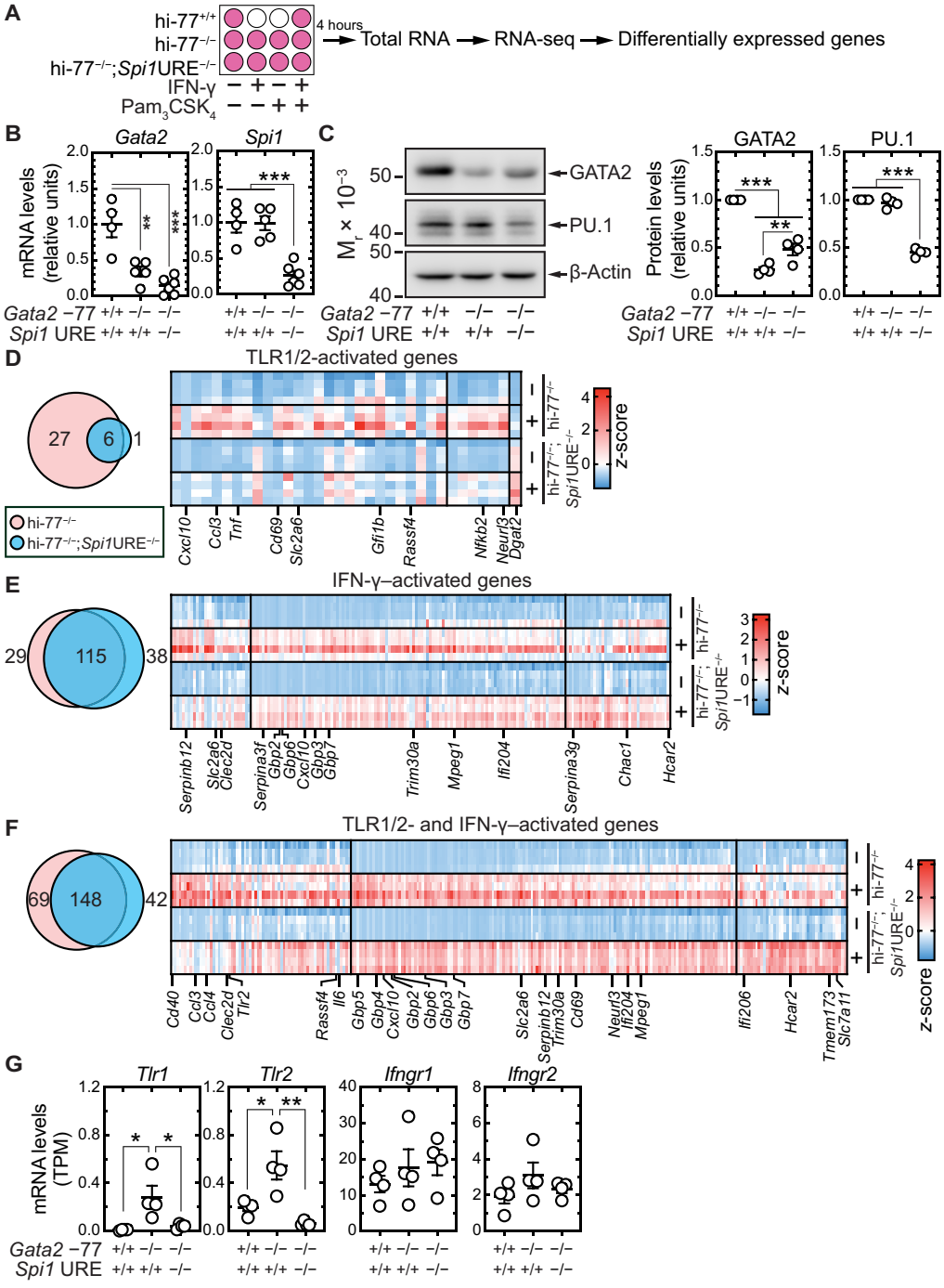

Fig. 3. Genome sensing of inflammatory stimuli in GATA2^{low} progenitors. (**A**) Strategy for gene expression analysis in ER-HOXB8–immortalized (hi) fetal liver myeloid progenitors. Wild-type (hi-77$^{+/+}$), GATA2^{low} (hi-77$^{-/-}$), and GATA2/PU.1^{low} (hi-77$^{-/-}$;*Spi1*URE$^{-/-}$) progenitors were treated with vehicle, IFN-γ (1 ng/ml), Pam_3CSK_4 (100 ng/ml), or both for 4 hours ($n = 4$ to 6 biological replicates). Total RNA was isolated for RNA-seq. (**B**) RT-qPCR analysis of *Gata2* and *Spi1* expression ($n = 4$ to 6 biological replicates). (**C**) Left: Representative Western blot of GATA2 and PU.1 expression. β-Actin was used as a loading control. Right: Densitometric analysis of band intensities normalized to β-Actin ($n = 4$). M_r is the apparent molecular mass in kDa. Statistics in (B) and (C): One-way ANOVA with Tukey's multiple comparisons test. $^*P < 0.05$; $^{**}P < 0.01$; $^{***}P < 0.001$. (**D**) Left: Overlap of activated differentially expressed genes (DEGs) in hi-77$^{-/-}$ and hi-77$^{-/-}$;*Spi1*URE$^{-/-}$ cells in response to Pam_3CSK_4. A DEG had $|\log_2(\text{fold change})| \geq 1$, adjusted *P*-value <0.05, and transcripts per million (TPM) ≥ 1 in all replicates in at least one of the two conditions compared. Right: Heatmap depicting expression of activated DEGs in response to Pam_3CSK_4 and presented as *z*-scores of TPMs. Representative genes are indicated. (**E**) Left: Overlap of activated DEGs in hi-77$^{-/-}$ and hi-77$^{-/-}$;*Spi1*URE$^{-/-}$ cells in response to IFN-γ. Right: Heatmap depicting expression of activated DEG in response to IFN-γ and presented as *z*-scores of TPMs. (**F**) Left: Overlap of activated DEGs in hi-77$^{-/-}$ and hi-77$^{-/-}$;*Spi1*URE$^{-/-}$ cells in response to IFN-γ and Pam_3CSK_4. Right: Heatmap depicting expression of activated DEGs upon combinatorial signaling and presented as *z*-scores of TPMs. Each section of the heatmaps in (D) and (E) corresponds to each section of Venn diagrams in the same order. (**G**) TLR gene (*Tlr1* and *Tlr2*) and IFN-γ receptor subunit (*Ifngr1* and *Ifngr2*) expression in GATA2^{low} and GATA2/PU.1^{low} progenitors.

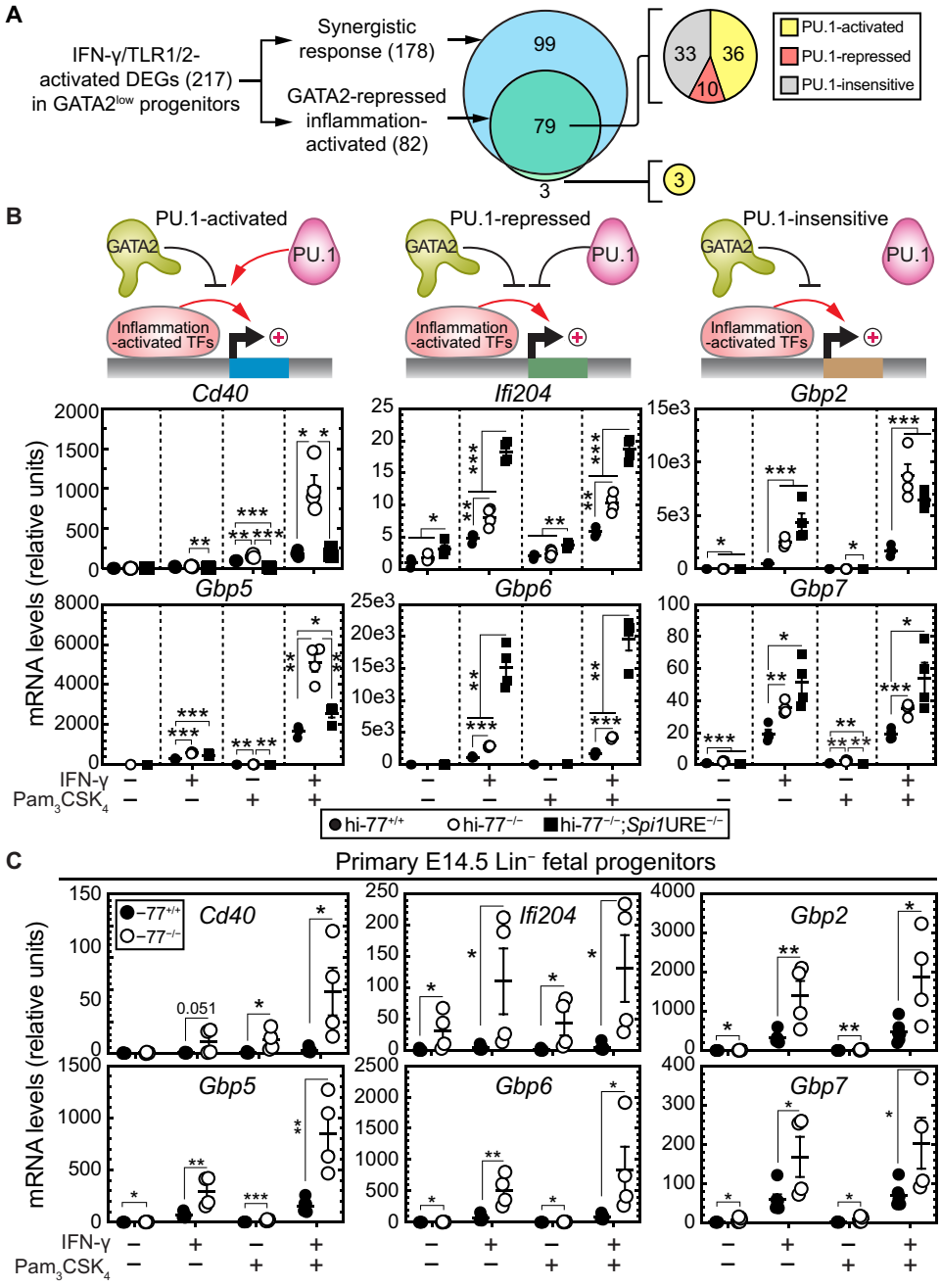

Fig. 4. Molecular determinants of inflammation-activated transcriptional responses. (**A**) GATA2-repressed genes that were activated synergistically in hi-$77^{-/-}$ cells by IFN-γ and Pam_3CSK_4 were parsed into PU.1-activated, PU.1-repressed, and PU.1-insensitive cohorts. The synergistic genes were defined as inflammation-activated DEGs with a larger $|\log_2(\text{fold change})|$ in combination versus vehicle than that of IFN-γ versus vehicle and Pam_3CSK_4 versus vehicle. (**B**) Top: Models depicting three different modes of regulation of signal-dependent genes by GATA2 and PU.1. Bottom: RT-qPCR analysis of representative synergistic genes with different GATA2/PU.1 regulatory modes was quantitated with RT-qPCR ($n = 4$). (**C**) The responsiveness of prioritized synergistic genes in primary lineage-depleted progenitors isolated from E14.5 fetal livers of $-77^{+/+}$ ($n = 6$) and $-77^{-/-}$ ($n = 4$) embryos (pooled from three litters). Statistics in (B) and (C): Multiple unpaired *t* tests. $^*P < 0.05$; $^{**}P < 0.01$; $^{***}P < 0.001$.

activation, repression, or insensitivity revealed cohorts with unique behaviors (Fig. 4B).

Tumor Necrosis Factor Receptor Superfamily Member 5 (*Cd40* or *Tnfrsf5*), which was highly activated by inflammation in hi-$77^{-/-}$ versus hi-$77^{+/+}$ cells, exemplifies a GATA2-repressed, PU.1-activated gene that responds synergistically to the two factors. In a proteomic study, the ligand of CD40 receptor (CD40L) was detected in serum of patients with GATA2 Deficiency Syndrome (*14*). Reducing PU.1 by ~50% attenuated *Cd40* expression to levels resembling hi-$77^{+/+}$ cells (Fig. 4B). By contrast, the IFN-activated, GATA2-repressed gene *Ifi204* was elevated further in hi-$77^{-/-}$;*Spi1*$URE^{-/-}$ versus hi-$77^{-/-}$ cells, indicating a PU.1-dependent repression mechanism

(Fig. 4B). Members of the Guanylate-binding protein (Gbp) family are IFN-inducible genes encoding proteins that protect cells from pathogens (*40*, *41*). GATA2 represses, and IFN-γ and TLR synergistically induce *Gbp* genes. *Gbp5* encodes an activator of NLRP3 inflammasome assembly (*41*), and, resembling *Cd40*, PU.1 promotes the transcriptional response (Fig. 4B). PU.1 repressed *Gbp6*, which was expressed in hi-77$^{-/-}$;*Spi1*URE$^{-/-}$ cells greater than hi-77$^{-/-}$ cells (Fig. 4B). Reducing PU.1 did not affect inflammation-induced *Gbp2* and *Gbp7* expression (Fig. 4B). Inflammation responsiveness of these genes was also detected in primary Lin^{-} progenitors from −77$^{+/+}$ and −77$^{-/-}$ E14.5 fetal livers (Fig. 4C). These studies demonstrated that PU.1 mediates a subset of inflammation-induced transcriptional responses in GATA2^{low} progenitors.

Mechanisms underlying genome sensing of inflammation

How does PU.1 mediate IFN-γ– and TLR-regulated genomic responses in GATA2^{low} progenitors? PU.1 might occupy inflammation-regulated loci independent of inflammation, with signal-dependent steps occurring post–chromatin occupancy. Alternatively, PU.1 might be excluded from loci in the steady state, and inflammation might promote PU.1 chromatin occupancy. We tested these models using cleavage under target and tagmentation (CUT&Tag) (*42*, *43*) to establish GATA2 and PU.1 chromatin occupancy in hi-77$^{+/+}$, hi-77$^{-/-}$, and hi-77$^{-/-}$;*Spi1*URE$^{-/-}$ cells without or with inflammation (Fig. 5A). H3K4me3 was used to detect active promoters (*44*, *45*), with immunoglobulin G (IgG) as a negative control. To establish whether GATA2 deficiency affects GATA2 and PU.1 chromatin occupancy, we compared the average of normalized CUT&Tag signals from −2 kb upstream of the transcription start site (TSS) to 1 kb downstream of the 3′-end of the gene at 217 inflammation-induced DEGs with hi-77$^{+/+}$, hi-77$^{-/-}$, and hi-77$^{-/-}$;*Spi1*URE$^{-/-}$ cells. GATA2 occupancy was detected in hi-77$^{+/+}$ cells and reduced in GATA2^{low} hi-77$^{-/-}$ cells (fig. S3A). Lowering PU.1 in hi-77$^{-/-}$ restored GATA2 occupancy to levels resembling wild type. Thus, PU.1 restricts GATA2 occupancy. PU.1 occupancy was indistinguishable in all cell types (fig. S3A).

To determine whether inflammation influences PU.1 chromatin occupancy in GATA2^{low} progenitors, we compared PU.1 CUT&Tag median signals at 217 inflammation-activated loci in hi-77$^{-/-}$ progenitors without or with inflammation (Fig. 5B). Because the PU.1 CUT&Tag signals were highest near the TSS (fig. S3A), we analyzed PU.1 occupancy from 1 kb upstream to 1 kb downstream of the TSS. This analysis revealed that inflammation increased PU.1 occupancy at 53 loci (Fig. 5, B and C). By averaging PU.1 signals from four biological replicates, the range of signals at these loci in inflammation-treated hi-77$^{-/-}$ progenitors was higher than the unstimulated control (Fig. 5D). Among 217 inflammation-activated loci, PU.1 occupied 87 genes, and inflammation did not affect occupancy (Fig. 5, B to D). PU.1 occupancy was undetectable at 77 loci regardless of inflammation, suggesting that PU.1 regulates transcription at these loci indirectly, or occupancy cannot be detected (Fig. 5, B and D, and fig. S3B). We also conducted the analysis using ranges from 0.5, 1, 2, and 5 kb surrounding the TSS. The 0.5- and 2-kb interval analyses revealed results resembling the 1-kb interval (fig. S3C). The 5-kb interval analysis revealed smaller PU.1 CUT&Tag signals with a reduced signal to noise. However, this analysis also identified genes with inflammation-induced versus inflammation-independent PU.1 occupancy. Using these gene cohorts, we asked whether inflammation influences GATA2 occupancy. By comparing the median of GATA2 CUT&Tag signals between unstimulated versus inflammation-treated hi-77$^{+/+}$ cells, inflammation increased GATA2 occupancy at most genes with inflammation-increased PU.1 occupancy (Fig. 5, B and D, and fig. S4A). Similarly, GATA2 preoccupied most genes with PU.1, and inflammation increased GATA2 occupancy.

As *Cd40* and *Gbp5* exemplify inflammation-induced genes activated synergistically by IFN-γ and TLR1/2 (Fig. 4, B and C), we tested how inflammation affected GATA2 and PU.1 occupancy at these loci. In the steady state, GATA2 and PU.1 did not occupy *Cd40* and *Gbp5* (Fig. 5E). Inflammation induced GATA2 and PU.1 occupancy at the promoters in hi-77$^{+/+}$ and hi-77$^{-/-}$ progenitors (Fig. 5, C and E). The ~75% reduction in GATA2 resulting from −77 enhancer deletion (hi-77$^{-/-}$, Fig. 3C) increased PU.1 occupancy relative to hi-77$^{+/+}$, and the ~50% PU.1 reduction in hi-77$^{-/-}$;*Spi1*URE$^{-/-}$ (Fig. 3C) reduced PU.1 occupancy to resemble wild-type (Fig. 5E). H3K4me3 was enriched at active promoters, complementing the *Cd40* and *Gbp5* expression data. Inflammation increased H3K4me3 in hi-77$^{+/+}$ and hi-77$^{-/-}$ cells, and lowering PU.1 reduced H3K4me3 in response to inflammation (Fig. 5E). Inflammation is, therefore, required for GATA2 and PU.1 to occupy an inflammation-activated gene cohort (Fig. 5F).

Ccl3 and *Cd69* exemplify inflammation-activated genes prebound by PU.1 (Fig. 5C). *Ccl3* encodes Macrophage Inflammatory Protein-1 alpha, which is elevated in patients with myeloproliferative neoplasm (*46*, *47*), and *Cd69* encodes a membrane protein important in lymphocytes (*48*, *49*). In the steady state, GATA2 and PU.1 occupied *Ccl3* and *Cd69* promoters, and inflammation did not affect GATA2 and PU.1 occupancy in wild-type progenitors (Fig. 5E). GATA2 deficiency reduced GATA2 and elevated PU.1 occupancy at these loci, and lowering PU.1 restored GATA2 and PU.1 occupancy to wild-type levels (Fig. 5E). GATA2 deficiency elevated PU.1 occupancy at the *Ccl3* promoter, and lowering PU.1 decreased PU.1 occupancy to levels resembling wild-type. Thus, GATA2 and PU.1 occupy select inflammation-activated loci independent of inflammation, and inflammation-activated transcription occurs post–chromatin occupancy at these loci (Fig. 5G).

What attributes distinguish the two modes of GATA2 and PU.1 function vis-à-vis inflammation-induced transcription? Comparing the magnitude of inflammation-induced transcription at genes exhibiting inflammation-induced PU.1 occupancy with PU.1-prebound genes revealed that genes regulated to the greatest extent exhibited inflammation-induced PU.1 occupancy (Fig. 5C and fig. S4B). By contrast, most PU.1-prebound genes were less responsive to inflammation (Fig. 5C and fig. S4B). We hypothesized that chromatin at prebound loci is accessible, and these loci are active in the basal state without inflammation, although inflammation increased transcription. Chromatin at loci in which inflammation increases PU.1 occupancy would be inaccessible in the basal state, and these loci would require inflammation for transcription. To test this hypothesis, we analyzed chromatin accessibility in hi-77$^{+/+}$ and GATA2^{low} progenitors using our previously described Assay for Transposase-Accessible Chromatin using sequencing (ATAC-seq) data (GSE201968) (*7*). Comparing accessibility of the top 10 genes [based on RNA-seq $\log_2$(fold change)] with inflammation-induced PU.1 occupancy to the top 10 PU.1-prebound genes revealed 9 of the 10 genes in the former group had closed chromatin in GATA2^{low} progenitors (ATAC-seq signals < 0.5 in four replicates); the sole exception was *Cd40* (Fig. 6A). By contrast, 9 of the 10 PU.1-prebound genes (except *Ifi47*) exhibited open chromatin in the basal state in GATA2^{low}

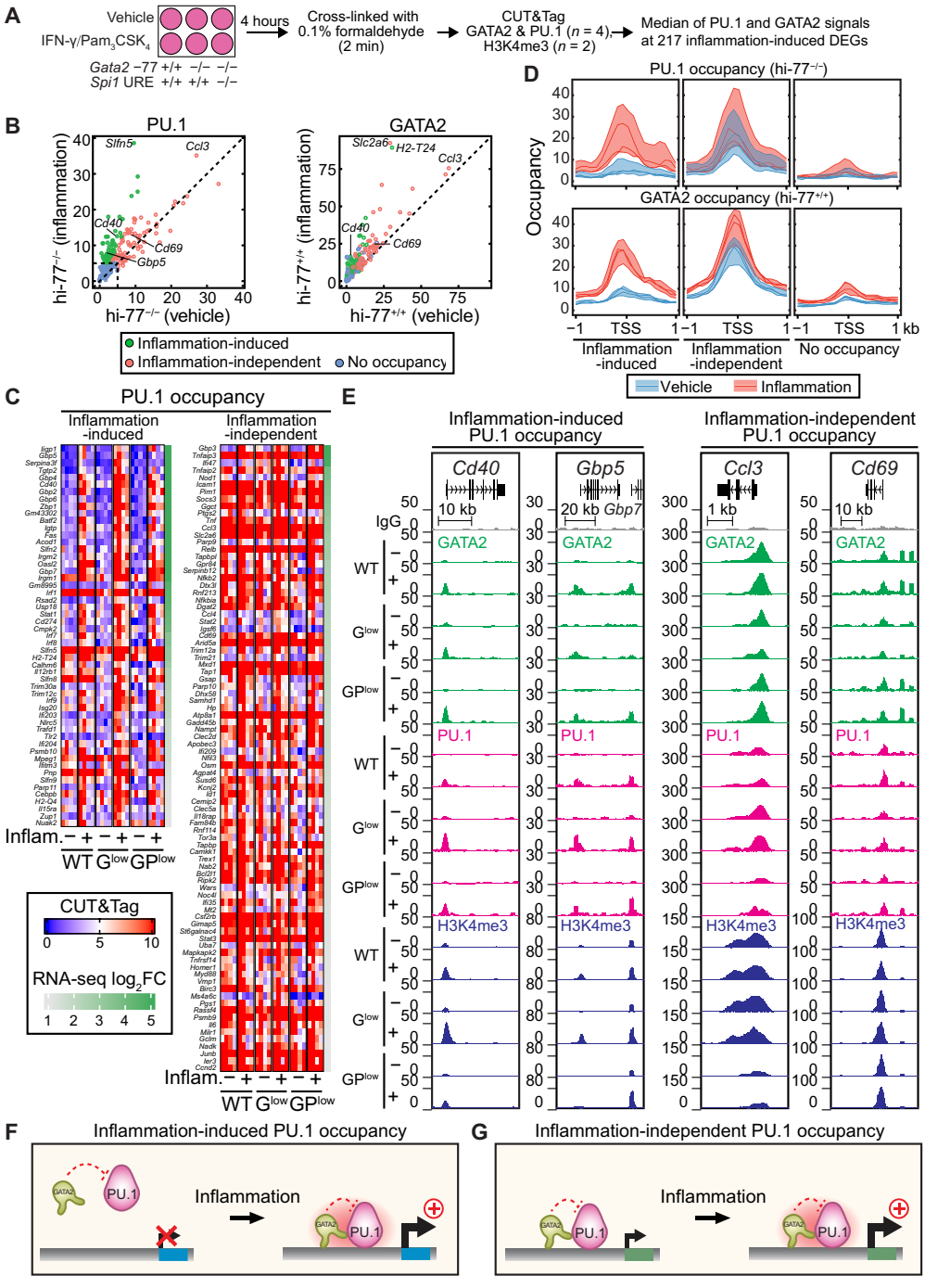

Fig. 5. Locus-specific mechanisms of inflammation-sensing in GATA2^{low} progenitors. (**A**) Schematic depicting the chromatin occupancy analysis. hi-77$^{+/+}$, hi-77$^{-/-}$, and hi-77$^{-/-}$;*Spi1*URE$^{-/-}$ cells were stimulated with vehicle or IFN-γ (1 ng/ml) and Pam_3CSK_4 (100 ng/ml) for 4 hours. Cells were cross-linked with 0.1% formaldehyde for 2 min before CUT&Tag analysis with antibodies against GATA2 ($n = 4$), PU.1 ($n = 4$), or H3K4me3 ($n = 2$). IgG with hi-77$^{+/+}$ served as a negative control. (**B**) Comparison of median PU.1 (left) and GATA2 (right) CUT&Tag signals at 217 DEGs in untreated versus inflammation-activated hi-77$^{-/-}$ and hi-77$^{+/+}$ cells, respectively. DEGs were colored by their cluster identities. The median signal is the median of signals from 1 kb upstream to 1 kb downstream of the transcription start site (TSS) of each DEG ($n = 4$). (**C**) Heatmaps depicting PU.1 CUT&Tag signals in untreated versus inflammation-treated hi-77$^{+/+}$ (WT), hi-77$^{-/-}$ (G^{low}), and hi-77$^{-/-}$;*Spi1*URE$^{-/-}$ (GP^{low}) progenitors. A total of 217 DEGs were clustered as inflammation-activated and inflammation-independent and ranked by their $\log_2$(fold change) on the basis of RNA-seq data of hi-77$^{-/-}$ (inflammation) versus hi-77$^{-/-}$ (vehicle). FC, fold change. (**D**) Range of signals for three categories of DEGs. The range is defined by the average signals of the four replicates from the same condition and presented as lines in the figure. Average signals are calculated over (TSS − 1 kb, TSS + 1 kb) with a bin width of 100 bp. (**E**) Representative CUT&Tag profiles (replicate 2) for genes with inflammation-induced GATA2 and PU.1 occupancy (*Cd40* and *Gbp5*) and genes prebound by GATA2 and PU.1 (*Ccl3* and *Cd69*). (**F**) Model of signal-dependent GATA2 and PU.1 occupancy at loci in GATA2^{low} progenitors. (**G**) Model depicting inflammation-independent GATA2 and PU.1 occupancy at inflammation-activated genes.

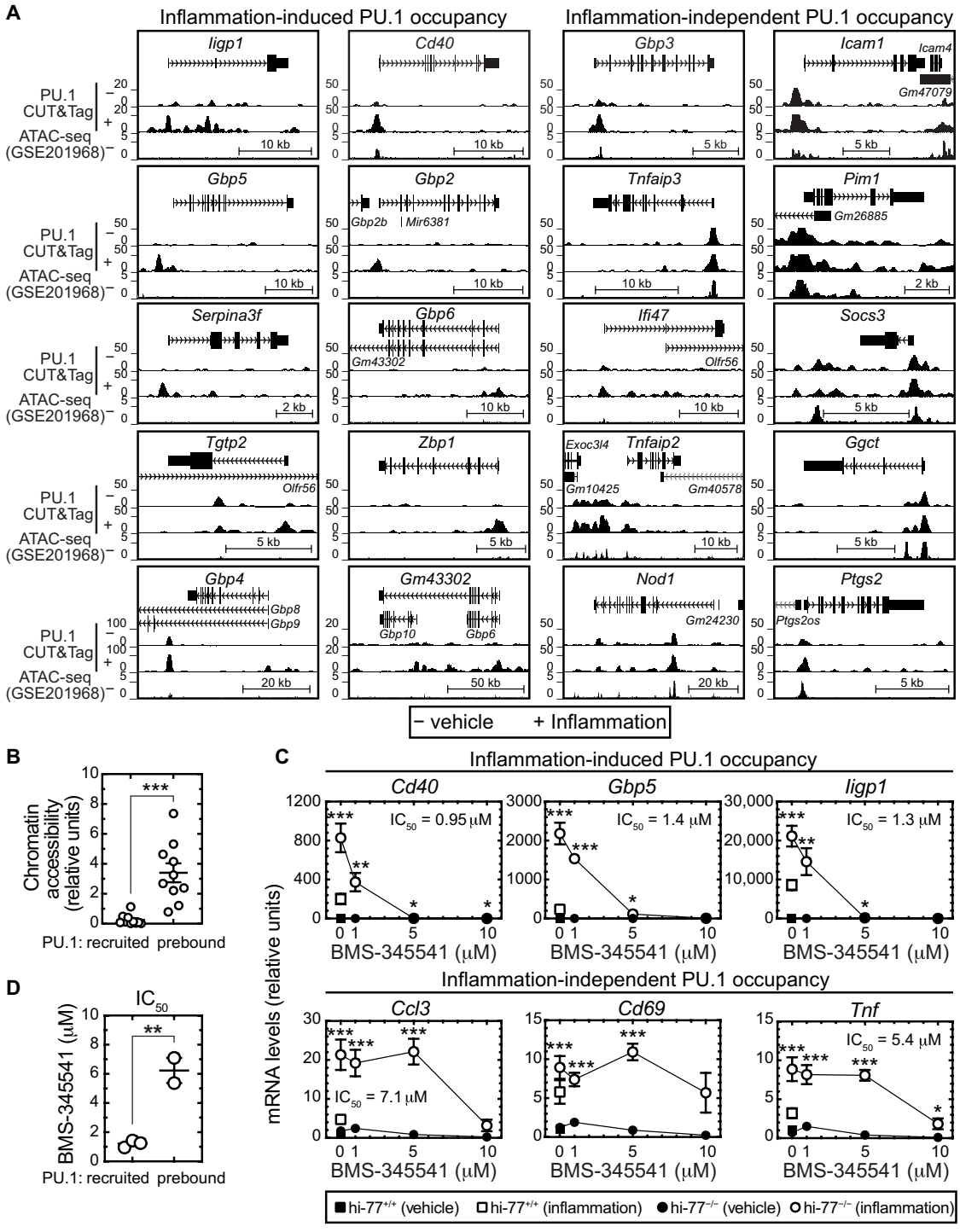

Fig. 6. Distinct molecular hallmarks of inflammation-activated genes with inflammation-induced or inflammation-independent PU.1 occupancy. (**A**) ATAC-seq profiles depicting chromatin accessibility of the top 10 genes with inflammation-induced (left) and inflammation-independent PU.1 occupancy (right). ATAC-seq profiles in hi-77$^{-/-}$ cells without inflammation were mined from published data (GSE201968) at loci harboring PU.1 occupancy (CUT&Tag replicate 2) in vehicle-treated (−) and inflammation-treated (+) hi-77$^{-/-}$ cells. (**B**) Comparison of average ATAC-seq signals from four biological replicates between genes with inflammation-induced PU.1 occupancy and genes with inflammation-independent PU.1 occupancy in (A). (**C**) Dose-response curve of three representative genes from inflammation-induced PU.1 occupancy and inflammation-independent PU.1 occupancy to IKK inhibitor BMS-345541. hi-77$^{-/-}$ progenitors were pretreated with increasing concentrations of BMS-345541 for 1 hour and treated with both IFN-γ (1 ng/ml) and Pam_3CSK_4 (100 ng/ml) for 4 hours ($n = 6$ biological replicates). hi-77$^{+/+}$ treated with or without both agents served as negative controls. Median inhibitory concentration (IC_{50}) for each gene was calculated using nonlinear regression. *Cd69* IC_{50} was uncalculated. (**D**) The IC_{50} of genes with inflammation-induced PU.1 occupancy was compared to those of genes with inflammation-independent occupancy. Individual values in (B) and (D) and means ± SEM in (B) to (D) were shown. Unpaired *t* test in (B) and (D) and multiple unpaired *t* test in (C). *$P < 0.05$; **$P < 0.01$; ***$P < 0.001$.

progenitors (Fig. 6A). The average ATAC-seq signal from the top 10 genes exhibiting inflammation-induced PU.1 occupancy was significantly ($P = 0.0002$) lower than the top 10 genes with inflammation-independent PU.1 occupancy (Fig. 6B). The top 10 genes with inflammation-induced PU.1 occupancy were not expressed in the steady state (fig. S4C) and had increased H3K4me3 upon inflammation (fig. S5). By contrast, the top 10 PU.1-prebound genes were expressed at varying levels in the basal state (fig. S4C). Among them, 9 of 10 had H3K4me3 in the uninduced state, and inflammatory signaling did not further increase H3K4me3 (fig. S5). *Ccl3* and *Cd69* promoters were active in the basal state, and inflammation did not affect H3K4me3 at these loci (Fig. 5E). Inflammation increased H3K4me3 at *Cd40* and *Gbp5* promoters, correlating with increased GATA2 and PU.1 occupancy upon inflammation (Fig. 5E and fig. S5). Thus, genes with inflammation-induced GATA2 and PU.1 occupancy are inaccessible in the steady state, and inflammation increases occupancy to activate transcription. At other loci, GATA2 and PU.1 preoccupied active genes, and inflammation further increased transcription. Many PU.1-prebound genes are located distally on chromosomes, and some reside in clusters, e.g., *Ccl* loci on chromosome 11 (fig. S6). Several *Gbp* family members exhibit inflammation-induced PU.1 occupancy and cluster on chromosome 3. The sex chromosomes are devoid of inflammation-activated genes, save *5430427O19Rik*, encoding TLR Adaptor Interacting with Endolysosomal SLC15A4 protein (*50*).

Because chromatin at PU.1-prebound genes without inflammation was more accessible than at genes with inflammation-induced PU.1 occupancy, presumably, other transcription factors and chromatin regulators are also prebound before inflammation. Genes with inflammation-induced PU.1 occupancy might require inflammation-activated transcription factors, e.g., NF-κB, for inflammation-dependent factor loading, while PU.1-prebound genes might not require inflammation-activated transcription factors for PU.1 occupancy, chromatin transitions, and/or activation. We asked whether antagonizing inflammation-induced NF-κB activation compromises the regulation of one or both gene cohorts. BMS-345541 binds IκB kinase (IKKβ) with a dissociation constant (K_d) of 130 nM while having a very low affinity for other kinases ($K_d > 1000$ nM) (*51*, *52*). GATA2^{low} progenitors were treated with increasing concentrations of BMS-345541 for 1 hour, followed by IFN-γ and Pam_3CSK_4 for 4 hours. hi-77$^{+/+}$ cells, with or without IFN-γ and Pam_3CSK_4, served as negative controls. Genes exhibiting inflammation-induced PU.1 occupancy (*Cd40*, *Gbp5*, and *Iigp1*) were very sensitive to BMS-345541 at 1 and 5 μM, whereas PU.1-prebound genes (*Ccl3*, *Cd69*, and *Tnf*) were insensitive to BMS-345541 at these concentrations (Fig. 6, C and D). As another IKKβ inhibitor, IKK16 (*53*), also distinguished the inflammation-activated gene cohorts (fig. S7), IKKβ activity is disproportionately important for the gene cohort requiring inflammation for PU.1 chromatin occupancy.

Inflammation reveals opposing functions of hematopoiesis-regulatory proteins

Our comparison of transcriptomes from progenitors with normal and reduced GATA2 levels revealed genes activated by inflammation in GATA2^{low} progenitors are enriched in motifs that bind signal-dependent transcription factors and RUNX motifs (*8*). To determine whether GATA2 antagonizes other transcription factors to regulate inflammation-induced transcription, we used Multiple Expectation Maximizations for Motif Elicitation (MEME) (*54*) to perform motif enrichment analysis at promoters and introns of inflammation-activated genes from our RNA-seq data (Fig. 7A). IFN-γ signaling uses members of the Signal Transducer and Activator of Transcription family and IRF family (*55*–*59*), while TLR signaling uses NF-κB to regulate transcription (*60*). Motifs that bind these factors were enriched at inflammation-activated genes (Fig. 7B and fig. S8, A and B). RUNX motifs were absent from promoters of genes activated in hi-77$^{+/+}$ and enriched in GATA2^{low} progenitors. RUNX motifs were not enriched at genes activated in hi-77$^{-/-}$;*Spi1*URE$^{-/-}$ progenitors (Fig. 7B). Find Individual Motif Occurrences (*61*) analysis revealed that, among 217 inflammation-activated DEGs in hi-77$^{-/-}$ cells, 70 genes harbored RUNX motifs in promoters. Motifs for the TAL-related factor NHLH1 (HEN1), DMRTB1, hairy-related factor BHLHE40 (BHE40), ETS factor ELK1, and NF-κB subunits were also enriched (Fig. 7B). RUNX1, RUNX2, and RUNX3 motifs were enriched in introns of hi-77$^{+/+}$, hi-77$^{-/-}$, and hi-77$^{-/-}$;*Spi1*URE$^{-/-}$ cells in response to inflammation. ELK1 and HEN1 motifs were enriched in introns of hi-77$^{-/-}$, but not hi-77$^{+/+}$ and hi-77$^{-/-}$;*Spi1*URE$^{-/-}$ cells (Fig. 7B). The progenitors expressed *Runx1*, but not *Elk1*, *Hen1*, *Runx2*, and *Runx3*.

Because RUNX1 and GATA2 can co-localize on chromatin, it is assumed that they function collectively (*62*–*64*). However, inflammation-activated genes harboring RUNX motifs were not induced in progenitors expressing normal GATA2 levels; the response was considerably stronger in GATA2^{low} progenitors, and RUNX motifs were not enriched when both GATA2 and PU.1 were reduced. We hypothesized that, in GATA2^{low} progenitors, RUNX1 functions in the inflammation-dependent activation mechanism. We tested whether RUNX1 in GATA2^{low} progenitors is required for IFN-γ– and TLR-mediated transcription by using CRISPR-Cas9 to ablate the common exon 2 of three *Runx1* isoforms in hi-77$^{-/-}$ cells, which abrogated RUNX1 mRNA and protein (Fig. 7, C to F). RUNX1 loss did not affect *Gata2* or *Spi1* expression (Fig. 7E). We treated hi-77$^{+/+}$, hi-77$^{-/-}$, and hi-77$^{-/-}$;*Runx1*$^{-/-}$ cells with IFN-γ and Pam_3CSK_4 for 4 hours and quantified the responsiveness of inflammation-activated genes. The GATA2-repressed chemokine genes *Ccl3* and *Ccl4* and cytokine gene *Tnf* were prebound by PU.1 and highly elevated in hi-77$^{-/-}$ versus hi-77$^{+/+}$ in response to signaling. RUNX1 loss attenuated activation of these genes to levels resembling hi-77$^{+/+}$ cells (Fig. 7G). *Ccl5* resides in a cluster with *Ccl3* and *Ccl4*, and its inflammation-induced expression in hi-77$^{-/-}$;*Runx1*$^{-/-}$ cells was also reduced to a wild-type level. This behavior resembled reducing PU.1 in GATA2^{low} progenitors (fig. S9A). By contrast, the responsiveness of PU.1-prebound gene *Cd69* was not affected by RUNX1 loss (Fig. 7G). Inflammation-induced activation of *Cd40* and *Iigp1*, whose PU.1 occupancy was inflammation-inducible, in hi-77$^{-/-}$ cells was unaffected when RUNX1 was deleted (Fig. 7G). However, *Cmpk2*, which encodes Cytidine/Uridine Monophosphate Kinase 2, exhibits inflammation-induced PU.1 chromatin occupancy, and RUNX1 loss attenuated its induction (Fig. 7G). On the basis of RUNX1 chromatin occupancy from CUT&RUN data obtained with murine bone marrow GMPs (*21*), RUNX1 occupied the *Ccl3* promoter, *Ccl4* (−3.7 kb), *Ccl5* (−19.9 kb), *Tnf* (+1.3 kb), and *Cmpk2* promoter and its −9-kb site (fig. S9B). RUNX1 occupancy was undetectable at *Cd40* and *Iigp1*, while RUNX1 occupied the *Cd69* promoter, intron 1, and −9.2-kb site (fig. S9C). Thus, loci exhibiting strong inflammation-induced transcription in GATA2^{low} progenitors were either sensitive or insensitive to RUNX1 loss. Because the inflammation response is high in GATA2^{low} cells and requires

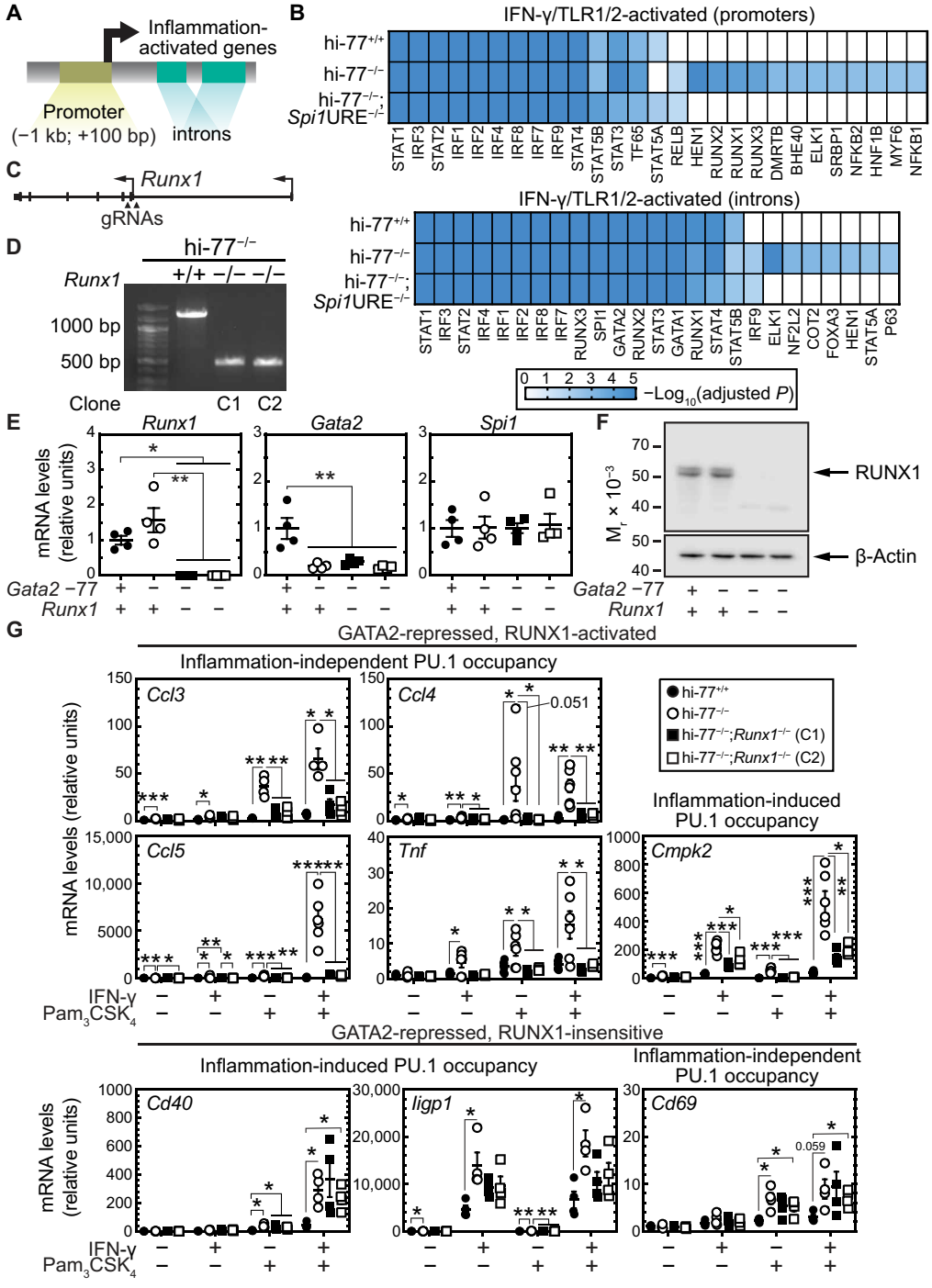

Fig. 7. Inflammation imparts opposing GATA2 and RUNX1 mechanisms. (**A**) Schematic of promoters and introns used for motif enrichment analysis of inflammation-activated genes. The promoter was defined as 1 kb upstream and 100 bp downstream of the TSS. (**B**) Heatmap showing motif enrichment, by MEME analysis, at promoters (top) and introns (bottom) of IFN-γ– and TLR-activated genes in hi-77$^{+/+}$, hi-77$^{-/-}$, and hi-77$^{-/-}$;*Spi1*URE$^{-/-}$ cells. Motifs binding canonical inflammation-activated transcription factors (STAT, IRF, and NF-κB) are presented as positive controls. Motifs enriched in hi-77$^{-/-}$ but not hi-77$^{+/+}$ or hi-77$^{-/-}$;*Spi1*URE$^{-/-}$ progenitors were ranked on the basis of $-\log_{10}$(*P* value) and a *P* value cutoff of 0.005. Motifs with adjusted *P* value > 0.05 were set to 1 Complete heatmaps of all enriched motifs were presented in fig. S8 (A and B). (**C**) Schematic depicting positions of guide RNA for CRISPR-Cas9 gene editing tool to delete *Runx1* gene in hi-77$^{-/-}$ progenitors. (**D**) PCR-based genotyping assay for *Runx1*$^{-/-}$ allele in hi-77$^{-/-}$ progenitors. Two hi-77$^{-/-}$;*Runx1*$^{-/-}$ clonal lines are denoted as C1 and C2. (**E**) *Runx1*, *Gata2*, and *Spi1* expression in hi-77$^{+/+}$, hi-77$^{-/-}$, and hi-77$^{-/-}$; *Runx1*$^{-/-}$ progenitors ($n = 4$). (**F**) Representative Western blot analysis of RUNX1 in hi-77$^{+/+}$, hi-77$^{-/-}$, and hi-77$^{-/-}$;*Runx1*$^{-/-}$ progenitors with β-Actin as a control. M_r is the apparent molecular mass in kDa. (**G**) The responsiveness of genes to IFN-γ and Pam_3CSK_4 was quantified using RT-qPCR. hi-77$^{+/+}$, hi-77$^{-/-}$, and hi-77$^{-/-}$;*Runx1*$^{-/-}$ progenitors were treated with or without IFN-γ (1 ng/ml), Pam_3CSK_4 (100 ng/ml), or both for 4 hours ($n = 4$ to 6). Statistics in (E) and (F): One-way ANOVA with Tukey's multiple comparisons test. *$P < 0.05$; **$P < 0.01$; ***$P < 0.001$.

RUNX1, GATA2 and RUNX1 exert opposing functions at these loci, which is not predictable from the co-localization, cooperativity paradigm.

Different molecular mechanisms governing progenitor genome sensing of qualitatively distinct inflammatory pathways

Prior studies revealed that RUNX1 loss in murine bone marrow GMP generated neutrophils with elevated TLR4 (*20*, *21*). Our results revealed that RUNX1 loss in GATA2^{low} progenitors attenuated responses to IFN-γ and TLR1/2 signaling at certain loci, which raised the question of whether GATA2 and RUNX1 are required for genome sensing of the same or different TLR signals. We tested this using CRISPR-Cas9 to ablate *Runx1* exon 2 in wild-type cells to generate hi-*Runx1*$^{-/-}$, which abrogated *Runx1* mRNA expression (Fig. 8, A and B). RUNX1 loss reduced *Gata2* expression by ~50% in both clonal lines without affecting *Spi1* expression (Fig. 8B). hi-77$^{+/+}$, hi-77$^{-/-}$, and hi-*Runx1*$^{-/-}$ progenitors were treated with TLR1/2 agonist Pam_3CSK_4 or TLR4 agonist LPS for 4 hours, and expression of inflammation-activated genes was quantified. GATA2 deficiency elevated *Ccl3* and *Ccl4* expression in the steady state versus wild-type, while RUNX1 loss reduced their expression (Fig. 8C). Thus, opposing activities of GATA2 and RUNX1 establish the transcription state of these loci. In response to TLR1/2 and TLR4, the six genes were elevated in GATA2^{low} cells. RUNX1-null cells were nonresponsive to the TLR1/2 agonist with all genes tested. However, RUNX1 loss increased expression of these genes in response to TLR4 agonist, with exceptions of *Ccl3* and *Ccl4* (Fig. 8C). GATA2

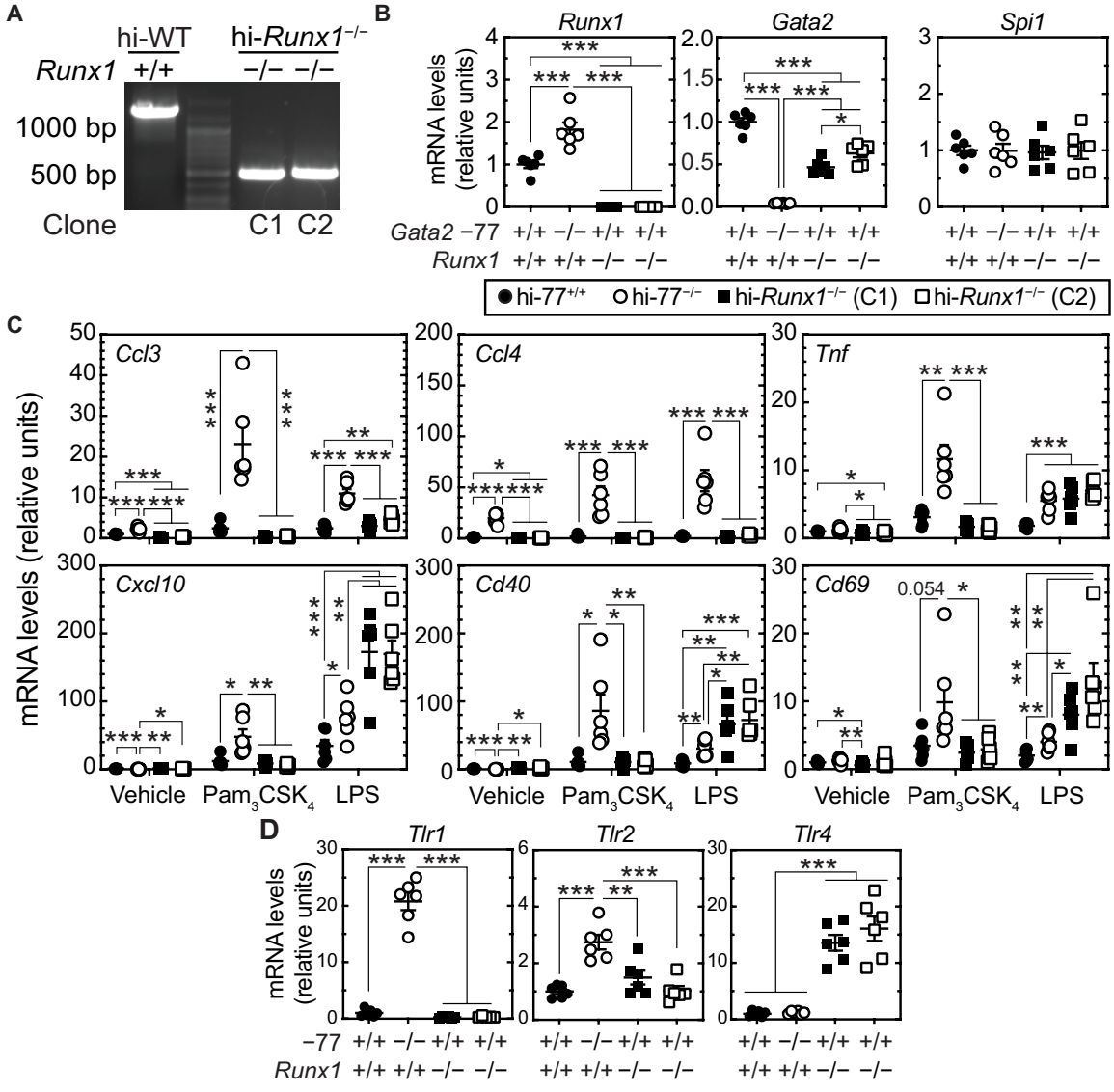

Fig. 8. Differential GATA2 and RUNX1 functions in genome sensing of qualitatively distinct inflammatory signals. (**A**) PCR-based genotyping assay for *Runx1*$^{-/-}$ allele in hi-77$^{+/+}$ progenitors. (**B**) *Runx1*, *Gata2*, and *Spi1* expression was quantified using RT-qPCR. (**C**) The responsiveness of select genes to TLR1/2 agonist (Pam_3CSK_4) and TLR4 agonist (LPS) were quantitated using RT-qPCR. hi-77$^{+/+}$, hi-77$^{-/-}$, and hi-*Runx1*$^{-/-}$ progenitors were treated with vehicle, Pam_3CSK_4 (100 ng/ml), or LPS (100 ng/ml) for 4 hours ($n = 6$ biological replicates). (**D**) *Tlr1*, *Tlr2*, and *Tlr4* expression in hi-77$^{+/+}$, hi-77$^{-/-}$, and hi-*Runx1*$^{-/-}$ progenitors was quantified using RT-qPCR. Statistics: One-way ANOVA with Tukey's multiple comparisons test. *$P < 0.05$; **$P < 0.01$; ***$P < 0.001$.

and RUNX1 are, therefore, differentially dedicated to controlling genome states that establish TLR1/2 versus TLR4 signaling, respectively.

To elucidate mechanisms underlying the differential sensitivity to TLR agonists, we compared the consequences of GATA2 or RUNX1 loss for *Tlr1*, *Tlr2*, and *Tlr4* expression. GATA2 deficiency elevated *Tlr1* 21-fold ($P < 0.0001$) and *Tlr2* 2.7-fold ($P < 0.0001$) without affecting *Tlr4* expression relative to wild type (Fig. 8D). While RUNX1 loss did not affect *Tlr1* and *Tlr2* expression, it increased *Tlr4* expression 14- and 16-fold ($P < 0.0001$) in both clonal lines (Fig. 8D), consistent with the prior report of RUNX1 suppressing *Tlr4* expression in neutrophils (*20*). The differential regulation of *Tlr* genes by GATA2 and RUNX1 may establish differential TLR1/2 versus TLR4-induced transcriptional responses.

DISCUSSION

Inflammation sensing by genomes reconfigures gene activity, enabling cells to adapt to microenvironment changes. For cells harboring a pathogenic genetic variant that amplifies the impact of inflammation on the genome, in principle, the exacerbated response may trigger pathogenesis. Although inflammatory mediators activate signal-dependent transcription factors, e.g., NF-κB or AP-1, that assemble complexes on enhancers and promoters, there are many unanswered questions on how qualitatively or quantitatively distinct permutations of inflammation impact genomes. Furthermore, the panoply of cytoplasmic and nuclear effectors that mediate inflammation-induced genome state changes is incompletely defined. Elucidating the mechanisms has high significance from fundamental and translational perspectives. We provide evidence for a genome-sensing paradigm involving antagonistic interactions between transcription factors not considered to be effectors of inflammation. This mechanism involved GATA2-PU.1 antagonism and GATA2-RUNX1 antagonism that occurred upon inflammation.

Our genomic analysis revealed inflammation-activated transcriptional mechanisms that differed at distinct genetic loci. Inflammation induced PU.1 occupancy at certain, but not all, inflammation-activated loci. Activation of loci with inflammation-induced PU.1 recruitment was exquisitely sensitive to pharmacological inhibitors of IKKβ kinase that phosphorylates IκB, leading to its destruction. The disproportionate IKKβ requirement for inflammation-activated transcription of loci exhibiting PU.1 recruitment versus loci with PU.1 occupancy preceding inflammation illustrates a critical locus-specific molecular step in inflammation sensing. IKKβ is required preferentially at inactive loci with closed chromatin that require PU.1 recruitment. By contrast, loci with prebound PU.1 and open chromatin were considerably less sensitive to IKKβ inhibitors. These loci were transcriptionally active without inflammation, and inflammation further activated transcription. These results define a dual mechanism of inflammation sensing by the genome of GATA2^{low} progenitors (Fig. 9), which was unpredictable from inflammation-induced transcriptional paradigms involving NF-κB and AP-1. In murine bone marrow–derived macrophages, TLR4 signaling induced NF-κB chromatin occupancy and nucleosome remodeling at inflammation-activated loci with inaccessible chromatin in the basal state (*65*). At loci accessible loci in the basal state, inflammation-activated genes harbored ETS motifs, although the specific ETS factor was not described. As our study analyzed regulatory complexes at and near promoters, it will be instructive to compare the results to analyses of broader genomic regions.

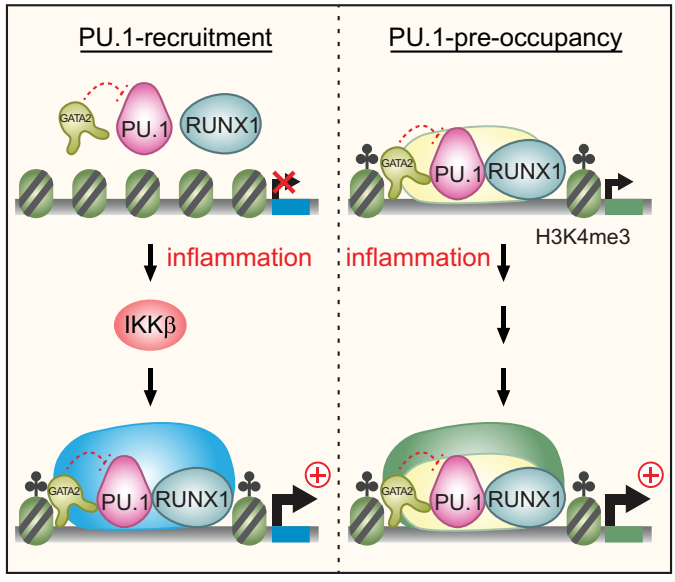

Fig. 9. Model for hematopoietic progenitor genome sensing of inflammation. The hematopoietic progenitor genome uses a dual PU.1-dependent mechanism to sense and respond to inflammation. A gene cohort has inaccessible chromatin in the steady state, and inflammation increases chromatin accessibility and occupancy of the hematopoietic transcription factors GATA2 and PU.1 to activate transcription via an IKKβ-dependent mechanism. At another inflammation-activated gene cohort, GATA2 and PU.1 occupancy precede inflammation, and this mechanism is not compromised by IKKβ inhibition. RUNX1 co-occupies chromatin with GATA2 and PU.1, yet GATA2 and RUNX1 differentially control inflammation-activated transcription, and transcriptional responses involving distinct TLR signaling pathways activated by unique pathogen-associated molecular patterns (*82*).

Through its HSPC-intrinsic activities, GATA2 is a vital determinant of hematopoiesis (*66*, *67*). Unlike transcription factors in which collaborating factors and coregulators are well established, factors and coregulators co-localize with GATA2 on chromatin, but the functional ramifications are unclear. An ensemble of transcription factors (GATA2, SCL/TAL1, RUNX1, FLI1, ERG, LYL1, and LMO2) termed the heptad complex co-localize and may function cooperatively (*62*, *64*, *68*). Although GATA2-occupied sites with multifactor occupancy are often enriched with motifs that bind heptad factors, previously, we demonstrated a reciprocal enrichment of WGATAR versus ETS and RUNX motifs at GATA2-repressed loci (*7*). Herein, we demonstrated that RUNX motifs were only enriched at promoters of inflammation-activated genes in GATA2^{low} progenitors and not when PU.1 was reduced. Lowering RUNX1 in GATA2^{low} progenitors revealed opposing activities of GATA2 and RUNX1 to confer inflammation-activated transcription in a locus-specific manner, which was unpredictable from existing paradigms.

It is instructive to consider the implications of opposing versus cooperative molecular functions of GATA2 and RUNX1 and, more broadly, how inflammation creates or enables mechanisms not operational in a "normal" context. With a cooperativity model, perturbations of factors in a complex would yield common consequences. Pathogenic *GATA2* and *RUNX1* variants share the consequence of creating bone marrow failure and leukemia predisposition, yet *GATA2* and *RUNX1* aberrations yield diseases with distinct clinical phenotypes. While *GATA2* genetic variants cause GATA2 Deficiency Syndrome with monocyte, dendritic cell, B cell, and natural killer cell

cytopenias (*69*–*73*), *RUNX1* variants cause RUNX1 Familial Platelet Disorder (*22*, *23*, *74*, *75*). As GATA2 regulates megakaryopoiesis (*76*), the differential phenotypes do not reflect the simple model that RUNX1, but not GATA2, has megakaryopoiesis-regulatory activity. Conceptually resembling GATA2^{low} progenitors, in which inflammation hyperactivates cytokine/chemokine gene expression, RUNX1 loss elevates transcriptional responses to inflammation in neutrophils (*20*, *21*). Unexpectedly, our study revealed that GATA2 and RUNX1 are vital for transcriptional responses to distinct inflammatory pathways: GATA2 for TLR1/2 and RUNX1 for TLR4.

Our study used GATA2^{low} fetal progenitors, and GATA2 loss elevates inflammatory genes in primary and immortalized fetal progenitors (*6*, *8*). In an AML mouse model harboring a compound *Nras*$^{G12D/+}$;*p53*$^{R172H/+}$ mutation, GATA2 was reduced in bone marrow HSPCs versus wild type, which correlated with up-regulated inflammatory genes, e.g., *Tlr1* and *Il6ra* (*77*). These results complement our finding that GATA2^{low} fetal progenitors elevate expression of inflammatory genes via PU.1-dependent and IKKβ-dependent or IKKβ-independent mechanisms, rendering progenitors hypersensitive to inflammatory mediators.

In summary, our study elucidated how the hematopoietic progenitor genome senses and responds to inflammation. GATA2 deficiency derepresses PU.1 activity, and inflammation induces PU.1 chromatin occupancy at a target gene cohort, while PU.1 constitutively occupies another cohort. Introducing IKKβ into GATA2 mechanisms and demonstrating that inflammation creates an antagonistic relationship between two hematopoiesis-promoting transcription factors, GATA2 and RUNX1, adds mechanistic depth to unravel how pathogen-instigated inflammation and inflammation of chronic disease alter HSPC functions. This mechanistic framework will enable studies to assess whether remodeling genome function yields adaptations that confer environmental protection and/or create vulnerabilities that trigger and/or accelerate progression of blood disease predisposition states.

MATERIALS AND METHODS

Mouse models and husbandry

The generation of *Gata2* $-77^{+/-}$ mice was previously described (*29*). *Myd88*$^{-/-}$ mice were purchased from the Jackson Laboratory (009088). These mice were crossed to generate *Gata2* $-77^{+/-}$;*Myd88*$^{-/-}$ mice for timed matings. The animal protocol was approved by the Institutional Animal Care and Use Committee at the University of Wisconsin-Madison with the approval number M005602, following the regulations from the Association for Assessment and Accreditation of Laboratory Animal Care International. Timed matings were performed using 8- to 18-week-old female mice.

Cell culture

hi-77$^{+/+}$, hi-77$^{-/-}$, and hi-77$^{-/-}$;*Spi1*URE$^{-/-}$ progenitor lines were previously generated and described (*7*). hi-77$^{-/-}$;*Runx1*$^{-/-}$ and hi-*Runx1*$^{-/-}$ progenitor lines were generated in this study using CRISPR-Cas9 tool. hi- cells were cultured in OPTI-MEM (31985-070, Thermo Fisher Scientific) supplemented with 10% fetal bovine serum (FBS; 100-106, GeminiBio), 1% penicillin-streptomycin (SV30079.01, Cytiva), 1% stem cell factor (SCF)–conditioned medium, 30 μM 2-mercaptoethanol (M3148, Sigma-Aldrich), 1 μM β-estradiol, and G418 (500 μg/ml; 400-111P-001, Gemini Bio). For cellular response analysis, ~200,000 cells were treated with vehicle [0.1% bovine serum albumin (A30075, Research Products International) in 1× phosphate-buffered saline (PBS)], IFN-γ (1 ng/ml; 315-05, PeproTech), TLR1/2 agonist Pam_3CSK_4 (tlrl-pms; 100 ng/ml; InvivoGen), or TLR4 agonist LPS (100 ng/ml; L2630, Sigma-Aldrich) for 4 hours. IKKβ inhibitors are from Selleckchem [BMS-345541 (S8044)] or a gift from S. Miyamoto (UW-Madison) [IKK16 (S2882)]. Data were pooled from at least two clonal lines for each cell (hi-77$^{+/+}$, hi-77$^{-/-}$, and hi-77$^{-/-}$;*Spi1*URE$^{-/-}$) or presented as two separate clonal lines (hi-77$^{-/-}$;*Runx1*$^{-/-}$ and hi-*Runx1*$^{-/-}$).

CRISPR-Cas9 gene editing

Guide sequences were designed by IDT tools (www.idtdna.com). CRISPR RNAs (crRNAs) [100 pmol; Integrated DNA Technologies (IDT)] were mixed with 200 pmol of trans-activating CRISPR RNA (tracrRNA) and incubated at 37°C for 30 min. Cas9 (8 μg; Aldevron) was added to the mixture and incubated at 37°C for 15 min. hi-77 cells (2×10^5) were resuspended in 20 μl of P3 buffer with 22% supplement (Lonza) and added to RNP complex. Electroporation was conducted with the EO-100 program on Nucleofector 4D (Lonza). After 72 hours, cells were seeded into 96-well plates (0.5 cells per well), cultured, and transferred to 24-well plates. Genotype the clones using polymerase chain reaction (PCR) assay. For homozygous mutant clones, the genomic DNA fragment including the deleted sequence was amplified by GoTaq DNA polymerase, cloned into the pBluescript vector, and sequenced.

Primary fetal progenitor cell isolation

The protocol was described previously (*78*). *Gata2* $-77^{+/-}$ and *Gata2* $-77^{+/-}$;*Myd88*$^{-/-}$ male and female mice were used for timed matings, and the presence of vaginal plug marked day 0.5. Pregnant females were sacrificed on day 14.5 with CO_2. Embryos were isolated on ice into Iscove's Modified Dulbecco's Medium, IMDM (12440-053, Gibco), containing 10% FBS. Genotyping was performed using fetal tails. The fetal livers were harvested into 1 ml of 1× PBS and 10% FBS. Cells were dissociated and counted using Trypan Blue (25-900-CI, Corning). Lineage depletion was performed using biotinylated-antibodies (CD3e, CD11b, CD19, CD45R, GR-1, CD71, and Ter119) (BioLegend) and MojoSort Streptavidin Nanobeads (BioLegend). Lineage-negative progenitors were cultured in IMDM containing 20% FBS, 4% SCF-conditioned medium, 4% interleukin-3–conditioned medium, and 1% penicillin-streptomycin. A total of 20,000 to 100,000 cells were treated with IFN-γ (1 ng/ml), TLR1/2 agonist Pam_3CSK_4 (100 ng/ml), or both agents for 4 hours to analyze gene responsiveness.

Flow cytometry and cell sorting

The cellular composition of E14.5 fetal liver was quantified using Attune (Thermo Fisher Scientific) flow cytometers, and CMPs and GMPs were sorted using FACSAria (BD Biosciences) as previously described (*30*). Unless specified, most antibodies were from BioLegend. Fluorescein isothiocyanate–conjugated B220 (103206), TER-119 (116206), CD3 (100306), CD5 (11-0193-85, Thermo Fisher Scientific), CD11b (101206), CD11c (117306), CD49b (108906), Ly6G (127606), and Sca1 (108106) antibodies were used for lineage exclusion. Other antibodies were Blue Violet (BV) 605–conjugated CD16/CD32 (563006, BD Biosciences), BV711-conjugated Ly6C (128017), phycoerythrin-conjugated CD115 (135506), eFluor 660–conjugated CD34 (50-0341, Thermo Fisher Scientific), peridinin chlorophyll-efluor710–conjugated CD135 (461351, Thermo Fisher Scientific), and phycoerythrin-Cy7–conjugated cKit (105814). Cells

were washed with ice-cold PBS containing 10% FBS and resuspended in 4′,6-diamidino-2-phenylindole (100 ng/ml) buffer for live-dead detection.

Gene expression analysis

The protocol was previously described (*8*). Cells were harvested and centrifuged at 2500 rpm for 5 min at 4°C to remove the supernatant. Cell pellets were dissociated in 50 μl of residual supernatant before adding 1 ml of TRIzol (Invitrogen). For a low number of cells (20,000 to 50,000), cells were kept overnight in the cold room to facilitate TRIzol digestion. Otherwise, cells were incubated in TRIzol for 10 min at room temperature. Total RNA was treated with deoxyribonuclease I (DNase I) (Invitrogen) for 15 min at room temperature, and DNase I was deactivated with EDTA at 65°C for 10 min. RNA was converted into cDNA in the mixture of primer cocktail [containing random hexamer and oligo(dT) primers], 5× First Strand Buffer, dithiothreitol, deoxyribonucleotide triphosphates dNTP, RNAsin, and MMLV reverse transcriptase (Invitrogen). cDNA was analyzed for genes of interest by real-time quantitative PCR (qPCR) using ViiA 7 Real-Time PCR cyclers (Applied Biosystems). Quantities were determined using standard curves and normalized to 18*S* control. Primer sequences were provided in table S1.

Western blot analysis

Following the published protocol (*8*), we harvested one million cells by centrifuging at 2500 rpm for 5 min at 4°C, washing with 1 ml of ice-cold PBS, resuspending in 50 μl of ice-cold PBS and 50 μl of 2× SDS sample buffer [50 mM tris, 2% β-mercaptoethanol, 2% SDS, 0.04% bromophenol blue, and 10% glycerol (pH 6.8)], and boiling for 10 min at 95°C. An equivalent of 100,000 cells was analyzed on 8% resolving gels by SDS–polyacrylamide gel electrophoresis, and proteins were transferred to a polyvinylidene difluoride membrane. Membranes were blocked with 5% milk in Tris-buffered saline containing Tween 20 (TBS-T) and incubated with primary antibodies overnight with gentle agitation in the cold room. GATA2 antibody was described previously (*79*). PU.1 (2258) and β-actin (3700) antibodies were from Cell Signaling Technology, and RUNX1 (sc-365644) antibody was from Santa Cruz Biotechnology. Proteins were detected and quantified with chemiluminescence (FEMTO Supersignal, Pierce) using LI-COR imaging instrument, and densitometry analysis was performed with Image Studio.

RNA sequencing

hi-$77^{-/-}$ and hi-$77^{-/-}$;*Spi1*URE$^{-/-}$ progenitors were treated with vehicle (0.1% bovine serum albumin in 1× PBS), IFN-γ, Pam_3CSK_4, or both agonists, and hi-$77^{+/+}$ progenitors were treated with or without both agonists for 4 hours. Four independent treatments for each condition were conducted. Total RNA was isolated using TRIzol and purified using the RNeasy MinElute Cleanup Kit (74204, Qiagen). The RNA library was prepared with Illumina TruSeq Stranded Total RNA (ribosomal RNA reduction) and sequenced using Illumina NovaSeq 6000 by the UW-Madison Gene Expression Center. Read alignment was performed by STAR (version 2.5.2b) to the mouse genome (version mm10). Gene expression levels were quantified by RSEM (version 1.3.0), and differential expression was determined with edgeR (version 3.36.0). A DEG was defined as having $|\log_2(\text{fold change})| \geq 1$, adjusted $P < 0.05$, and transcripts per million ≥ 1 in all the replicates in at least one of the two conditions. DEGs were divided into activated, which had higher expression in the numerator versus the denominator condition, and repressed, which had lower expression in the numerator versus the denominator condition. Motif analysis was conducted as previously described (*8*) with AME from MEME (version 5.3.3) on promoters and introns of DEGs. The promoters were defined as from 1 kb upstream of the TSS to 100 base pairs (bp) downstream of the TSS. The promoters and introns of protein-coding or lncRNA-expressing genes on chromosomes 1 to 19, X, or Y, were analyzed. Chromosome M was excluded. The promoters of IFN-γ/Pam_3CSK_4-activated DEGs in hi-$77^{-/-}$ progenitors were scanned for RUNX motifs with FIMO from MEME. Gene Expression Omnibus GEO accession number is GSE279155.

Cleavage under target and tagmentation

CUT&Tag was conducted as described (*42*, *43*, *80*). Concanavalin A magnetic beads (BP531, Bangs Laboratories) were activated by washing twice in binding buffer [20 mM Hepes (pH 7.9), 10 mM KCl, 1 mM $CaCl_2$, 1 mM $MnCl_2$, and 0.1% bovine serum albumin (BSA)]. hi-77 progenitors were gently cross-linked with 0.1% formaldehyde for 2 min and quenched with 75 mM glycine. Cells were washed twice in 1.5 ml of wash buffer [20 mM Hepes (pH 7.5), 150 mM NaCl, 0.83 mM spermidine, 0.1% BSA, and one Roche cOmplete Protease Inhibitor EDTA-free tablet] and resuspended in 1 ml of wash buffer. For four antibodies, 600,000 cells in 1 ml of final volume of wash buffer were mixed with 40 μl of activated bead suspension and rotated for 30 min at room temperature. On a magnetic rack, wash buffer was replaced with 600 μl of antibody buffer [wash buffer and digitonin (0.1 μg/ml) and 2 mM EDTA] and aliquoted into four tubes (150 μl each). Affinity-purified rabbit polyclonal anti-GATA2 antibody (1.2 μg) (*79*, *81*), anti-PU.1 mouse antibody (1.2 μg; Santa Cruz Biotechnology, sc-390405), H3K4me3 rabbit antibody (1 μg; Abcam, ab213224), or rabbit IgG isotype-matched control (1 μg; Invitrogen, 10500C) was added to each tube. Tubes were rotated overnight at 4°C. After a quick spin, tubes were replaced on a magnetic stand, and antibody buffer was replaced with 150 μl of Dig-Wash buffer [wash buffer and digitonin (0.1 μg/ml)] containing secondary antibody (1:100 dilution) for either rabbit or mouse antibody. After an hour on a Nutator at room temperature, cells were washed three times with dig-wash buffer. Resuspended cells in 150 μl of Dig-300 buffer [20 mM Hepes (pH 7.5), 300 mM NaCl, 0.83 mM spermidine, digitonin (0.1 μg/ml), 0.1% BSA, and one Roche cOmplete Protease Inhibitor EDTA-free tablet] containing pA-Tn5 preloaded with MEDS adapters (1:250 dilution). After nutating at room temperature for 1 hour, cells were washed three times with Dig-300 buffer. Added 300 μL tagmentation buffer (Dig-300 wash and 10 mM $MgCl_2$) and nutated tubes at 37°C for 1 hour. Cells were isolated by centrifugation, and 10 μl of 0.5 M EDTA was added to stop tagmentation, followed by addition of 3 μl of 10% SDS and 3 μl of proteinase K (20 mg/ml; New England Biolabs NEB, no. P8107S). Cells were incubated at 37°C overnight on a thermomixer at 600 rpm. DNA was purified by phenol-chloroform extraction and ethanol precipitation. DNA (1.31 μl) was analyzed by reverse transcription (RT)–qPCR in a 25-μl reaction containing 10 μM i5 and i7 primers and PowerUp SYBR Green Master Mix. Libraries were prepared with the NEB Next HiFi 2× PCR Master Mix (M0514S) following the manufacturer's protocol. The number of PCR cycles was determined on the basis of RT-qPCR. Sample concentration was determined using Qubit 1× dsDNA HS Assay (Thermo Fisher Scientific, Q33231). The quality of the library was assessed using Bioanalyzer High Sensitivity DNA Analysis (Agilent). Samples were

pooled and sequenced on NovaSeq 6000 using 50 bp paired-end sequencing at about 10 million reads per sample. CUT&Tag FASTQ files were processed by removing the adapter "CTGTCTCTTATACACATCT" using the Cutadapt software (version 4.5) and aligned to the mouse genome (version mm10) by Bowtie2 (version 2.5.1). Duplicated fragments were marked and removed by Picard (version 3.1.1). The CUT&Tag raw data were deposited to GEO with the accession number GSE279156.

Statistical analysis

Statistical analysis was performed using GraphPad Prism 10 (GraphPad, San Diego, CA, USA). The graphs were presented as means ± SEM. Outliers were identified using the Grubbs or Robust Regression and Outlier Updated Test (ROUT) test. The statistical tests and the number of biological replicates for each experiment are indicated in the figure legends.

Supplementary Materials

This PDF file includes:

Figs. S1 to S9
Table S1

REFERENCES AND NOTES

1. R. Medzhitov, The spectrum of inflammatory responses. *Science* **374**, 1070–1075 (2021).
2. Y. Mei, K. Ren, Y. Liu, A. Ma, Z. Xia, X. Han, E. Li, H. Tariq, H. Bao, X. Xie, C. Zou, D. Zhang, Z. Li, L. Dong, A. Verma, X. Lu, Y. Abaza, J. K. Altman, M. Sukhanova, J. Yang, P. Ji, Bone marrow-confined IL-6 signaling mediates the progression of myelodysplastic syndromes to acute myeloid leukemia. *J. Clin. Invest.* **132**, e152673 (2022).
3. T. Y. Zhang, R. Dutta, B. Benard, F. Zhao, R. Yin, R. Majeti, IL-6 blockade reverses bone marrow failure induced by human acute myeloid leukemia. *Sci. Transl. Med.* **12**, eaax5104 (2020).
4. M. Kleppe, M. Kwak, P. Koppikar, M. Riester, M. Keller, L. Bastian, T. Hricik, N. Bhagwat, A. S. McKenney, E. Papalexi, O. Abdel-Wahab, R. Rampal, S. Marubayashi, J. J. Chen, V. Romanet, J. S. Fridman, J. Bromberg, J. Teruya-Feldstein, M. Murakami, T. Radimerski, F. Michor, R. Fan, R. L. Levine, JAK-STAT pathway activation in malignant and nonmalignant cells contributes to MPN pathogenesis and therapeutic response. *Cancer Discov.* **5**, 316–331 (2015).
5. J. J. Trowbridge, D. T. Starczynowski, Innate immune pathways and inflammation in hematopoietic aging, clonal hematopoiesis, and MDS. *J. Exp. Med.* **218**, e20201544 (2021).
6. K. D. Johnson, D. J. Conn, E. Shishkova, K. R. Katsumura, P. Liu, S. Shen, E. A. Ranheim, S. G. Kraus, W. Wang, K. R. Calvo, A. P. Hsu, S. M. Holland, J. J. Coon, S. Keles, E. H. Bresnick, Constructing and deconstructing GATA2-regulated cell fate programs to establish developmental trajectories. *J. Exp. Med.* **217**, e20191526 (2020).
7. M. M. Jung, S. Shen, G. A. Botten, T. Olender, K. R. Katsumura, K. D. Johnson, A. A. Soukup, P. Liu, Q. Zhang, Z. D. Jensvold, P. W. Lewis, R. A. Beagrie, J. K. Low, L. Yang, J. P. Mackay, L. A. Godley, M. Brand, J. Xu, S. Keles, E. H. Bresnick, Pathogenic human variant that dislocates GATA2 zinc fingers disrupts hematopoietic gene expression and signaling networks. *J. Clin. Invest.* **133**, e162685 (2023).
8. V. L. Tran, P. Liu, K. R. Katsumura, E. Kim, B. M. Schoff, K. D. Johnson, E. H. Bresnick, Restricting genomic actions of innate immune mediators on fetal hematopoietic progenitor cells. *iScience* **26**, 106297 (2023).
9. K. R. Katsumura, C. Mehta, K. J. Hewitt, A. A. Soukup, I. Fraga de Andrade, E. A. Ranheim, K. D. Johnson, E. H. Bresnick, Human leukemia mutations corrupt but do not abrogate GATA-2 function. *Proc. Natl. Acad. Sci. U.S.A.* **115**, E10109–E10118 (2018).
10. K. R. Katsumura, C. Yang, M. E. Boyer, L. Li, E. H. Bresnick, Molecular basis of crosstalk between oncogenic Ras and the master regulator of hematopoiesis GATA-2. *EMBO Rep.* **15**, 938–947 (2014).
11. K. R. Katsumura, I. M. Ong, A. W. DeVilbiss, R. Sanalkumar, E. H. Bresnick, GATA factor-dependent positive-feedback circuit in acute myeloid leukemia cells. *Cell Rep.* **16**, 2428–2441 (2016).
12. K. R. Katsumura, P. Liu, J. A. Kim, C. Mehta, E. H. Bresnick, Pathogenic GATA2 genetic variants utilize an obligate enhancer mechanism to distort a multilineage differentiation program. *Proc. Natl. Acad. Sci. U.S.A.* **121**, e2317147121 (2024).
13. M. A. Spinner, L. A. Sanchez, A. P. Hsu, P. A. Shaw, C. S. Zerbe, K. R. Calvo, D. C. Arthur, W. Gu, C. M. Gould, C. C. Brewer, E. W. Cowen, A. F. Freeman, K. N. Olivier, G. Uzel, A. M. Zelazny, J. R. Daub, C. D. Spalding, R. J. Claypool, N. K. Giri, B. P. Alter, E. M. Mace, J. S. Orange, J. Cuellar-Rodriguez, D. D. Hickstein, S. M. Holland, GATA2 deficiency: A protean disorder of hematopoiesis, lymphatics, and immunity. *Blood* **123**, 809–821 (2014).
14. R. E. Dickinson, P. Milne, L. Jardine, S. Zandi, S. I. Swierczek, N. McGovern, S. Cookson, Z. Ferozepurwalla, A. Langridge, S. Pagan, A. Gennery, T. Heiskanen-Kosma, S. Hamalainen, M. Seppanen, M. Helbert, E. Tholouli, E. Gambineri, S. Reykdal, M. Gottfreethsson, J. E. Thaventhiran, E. Morris, G. Hirschfield, A. G. Richter, S. Jolles, C. M. Bacon, S. Hambleton, M. Haniffa, Y. Bryceson, C. Allen, J. T. Prchal, J. E. Dick, V. Bigley, M. Collin, The evolution of cellular deficiency in GATA2 mutation. *Blood* **123**, 863–874 (2014).
15. A. A. Soukup, D. R. Matson, P. Liu, K. D. Johnson, E. H. Bresnick, Conditionally pathogenic genetic variants of a hematopoietic disease-suppressing enhancer. *Sci. Adv.* **7**, eabk3521 (2021).
16. A. A. Soukup, E. H. Bresnick, Gata2 noncoding genetic variation as a determinant of hematopoietic stem/progenitor cell mobilization efficiency. *Blood Adv.* **7**, 7564–7575 (2023).
17. A. A. Soukup, Y. Zheng, C. Mehta, J. Wu, P. Liu, M. Cao, I. Hofmann, Y. Zhou, J. Zhang, K. D. Johnson, K. Choi, S. Keles, E. H. Bresnick, Single-nucleotide human disease mutation inactivates a blood-regenerative GATA2 enhancer. *J. Clin. Invest.* **129**, 1180–1192 (2019).
18. A. Yeaton, G. Cayanan, S. Loghavi, I. Dolgalev, E. M. Leddin, C. E. Loo, H. Torabifard, D. Nicolet, J. Wang, K. Corrigan, V. Paraskevopoulou, D. T. Starczynowski, E. Wang, O. Abdel-Wahab, A. D. Viny, R. M. Stone, J. C. Byrd, O. A. Guryanova, R. M. Kohli, G. A. Cisneros, A. Tsirigos, A. K. Eisfeld, I. Aifantis, M. Guillamot, The impact of inflammation-induced tumor plasticity during myeloid transformation. *Cancer Discov.* **12**, 2392–2413 (2022).
19. A. Rodriguez-Meira, R. Norfo, S. Wen, A. L. Chedeville, H. Rahman, J. O'Sullivan, G. Wang, E. Louka, W. W. Kretzschmar, A. Paterson, C. Brierley, J. E. Martin, C. Demeule, M. Bashton, N. Sousos, D. Moralli, L. Subha Meem, J. Carrelha, B. Wu, A. Hamblin, H. Guermouche, F. Pasquier, C. Marzac, F. Girodon, W. Vainchenker, M. Drummond, C. Harrison, J. R. Chapman, I. Plo, S. E. W. Jacobsen, B. Psaila, S. Thongjuea, I. Antony-Debre, A. J. Mead, Single-cell multi-omics identifies chronic inflammation as a driver of TP53-mutant leukemic evolution. *Nat. Genet.* **55**, 1531–1541 (2023).
20. D. C. Bellissimo, C. H. Chen, Q. Zhu, S. Bagga, C. T. Lee, B. He, G. B. Wertheim, M. Jordan, K. Tan, G. S. Worthen, D. G. Gilliland, N. A. Speck, Runx1 negatively regulates inflammatory cytokine production by neutrophils in response to Toll-like receptor signaling. *Blood Adv.* **4**, 1145–1158 (2020).
21. A. U. Zezulin, D. Yen, D. Ye, E. D. Howell, E. Bresciani, J. Diemer, J. G. Ren, M. H. Ahmad, L. H. Castilla, I. P. Touw, A. J. Minn, W. Tong, P. P. Liu, K. Tan, W. Yu, N. A. Speck, RUNX1 is required in granulocyte-monocyte progenitors to attenuate inflammatory cytokine production by neutrophils. *Genes Dev.* **37**, 605–620 (2023).
22. J. E. Churpek, E. H. Bresnick, Transcription factor mutations as a cause of familial myeloid neoplasms. *J. Clin. Invest.* **129**, 476–488 (2019).
23. W. J. Song, M. G. Sullivan, R. D. Legare, S. Hutchings, X. Tan, D. Kufrin, J. Ratajczak, I. C. Resende, C. Haworth, R. Hock, M. Loh, C. Felix, D. C. Roy, L. Busque, D. Kurnit, C. Willman, A. M. Gewirtz, N. A. Speck, J. H. Bushweller, F. P. Li, K. Gardiner, M. Poncz, J. M. Maris, D. G. Gilliland, Haploinsufficiency of CBFA2 causes familial thrombocytopenia with propensity to develop acute myelogenous leukaemia. *Nat. Genet.* **23**, 166–175 (1999).
24. M. Bloom, N. Oak, R. Baskin-Doerfler, R. Feng, I. Iacobucci, P. Baviskar, X. Zhao, A. N. Stroh, C. Li, P. Ozark, H. S. Tillman, Y. Li, K. C. Verbist, S. Albeituni, D. C. Scott, M. T. King, S. L. McKinney-Freeman, M. J. Weiss, J. J. Yang, K. E. Nichols, ETV6 represses inflammatory response genes and regulates HSPC function during stress hematopoiesis in mice. *Blood Adv.* **7**, 5608–5623 (2023).
25. M. Y. Zhang, J. E. Churpek, S. B. Keel, T. Walsh, M. K. Lee, K. R. Loeb, S. Gulsuner, C. C. Pritchard, M. Sanchez-Bonilla, J. J. Delrow, R. S. Basom, M. Forouhar, B. Gyurkocza, B. S. Schwartz, B. Neistadt, R. Marquez, C. J. Mariani, S. A. Coats, I. Hofmann, R. C. Lindsley, D. A. Williams, J. L. Abkowitz, M. S. Horwitz, M. C. King, L. A. Godley, A. Shimamura, Germline ETV6 mutations in familial thrombocytopenia and hematologic malignancy. *Nat. Genet.* **47**, 180–185 (2015).
26. J. C. Walsh, R. P. DeKoter, H.-J. Lee, E. D. Smith, D. W. Lancki, M. F. Gurish, D. S. Friend, R. L. Stevens, J. Anastasi, H. Singh, Cooperative and antagonistic interplay between PU.1 and GATA-2 in the specification of myeloid cell fates. *Immunity* **17**, 665–676 (2002).
27. J. C. Wheat, Y. Sella, M. Willcockson, A. I. Skoultchi, A. Bergman, R. H. Singer, U. Steidl, Single-molecule imaging of transcription dynamics in somatic stem cells. *Nature* **583**, 431–436 (2020).
28. A. Rein, I. Geron, E. Kugler, H. Fishman, E. Gottlieb, I. Abramovich, A. Giladi, I. Amit, R. Mulet-Lazaro, R. Delwel, S. Groschel, S. Levin-Zaidman, N. Dezorella, V. Holdengreber, T. N. Rao, J. Yacobovich, O. Steinberg-Shemer, Q. H. Huang, Y. Tan, S. J. Chen, S. Izraeli, Y. Birger, Cellular and metabolic characteristics of pre-leukemic hematopoietic progenitors with GATA2 haploinsufficiency. *Haematologica* **108**, 2316–2330 (2023).

29. K. D. Johnson, G. Kong, X. Gao, Y. I. Chang, K. J. Hewitt, R. Sanalkumar, R. Prathibha, E. A. Ranheim, C. N. Dewey, J. Zhang, E. H. Bresnick, Cis-regulatory mechanisms governing stem and progenitor cell transitions. *Sci. Adv.* **1**, e1500503 (2015).
30. K. D. Johnson, A. A. Soukup, E. H. Bresnick, GATA2 deficiency elevates interferon regulatory factor-8 to subvert a progenitor cell differentiation program. *Blood Adv.* **6**, 1464–1473 (2022).
31. A. Yáñez, M. Y. Ng, N. Hassanzadeh-Kiabi, H. S. Goodridge, IRF8 acts in lineage-committed rather than oligopotent progenitors to control neutrophil vs monocyte production. *Blood* **125**, 1452–1459 (2015).
32. T. Tamura, T. Nagamura-Inoue, Z. Shmeltzer, T. Kuwata, K. Ozato, ICSBP directs bipotential myeloid progenitor cells to differentiate into mature macrophages. *Immunity* **13**, 155–165 (2000).
33. H. Wesche, W. J. Henzel, W. Shillinglaw, S. Li, Z. Cao, MyD88: An adapter that recruits IRAK to the IL-1 receptor complex. *Immunity* **7**, 837–847 (1997).
34. M. Muzio, J. Ni, P. Feng, V. M. Dixit, IRAK (Pelle) family member IRAK-2 and MyD88 as proximal mediators of IL-1 signaling. *Science* **278**, 1612–1615 (1997).
35. R. Ostuni, V. Piccolo, I. Barozzi, S. Polletti, A. Termanini, S. Bonifacio, A. Curina, E. Prosperini, S. Ghisletti, G. Natoli, Latent enhancers activated by stimulation in differentiated cells. *Cell* **152**, 157–171 (2013).
36. S. Heinz, C. Benner, N. Spann, E. Bertolino, Y. C. Lin, P. Laslo, J. X. Cheng, C. Murre, H. Singh, C. K. Glass, Simple combinations of lineage-determining transcription factors prime cis-regulatory elements required for macrophage and B cell identities. *Mol. Cell* **38**, 576–589 (2010).
37. A. Mancino, A. Termanini, I. Barozzi, S. Ghisletti, R. Ostuni, E. Prosperini, K. Ozato, G. Natoli, A dual cis-regulatory code links IRF8 to constitutive and inducible gene expression in macrophages. *Genes Dev.* **29**, 394–408 (2015).
38. Y. Li, Y. Okuno, P. Zhang, H. S. Radomska, H. Chen, H. Iwasaki, K. Akashi, M. J. Klemsz, S. R. McKercher, R. A. Maki, D. G. Tenen, Regulation of the PU.1 gene by distal elements. *Blood* **98**, 2958–2965 (2001).
39. F. Rosenbauer, K. Wagner, J. L. Kutok, H. Iwasaki, M. M. Le Beau, Y. Okuno, K. Akashi, S. Fiering, D. G. Tenen, Acute myeloid leukemia induced by graded reduction of a lineage-specific transcription factor, PU.1. *Nat. Genet.* **36**, 624–630 (2004).
40. B.-H. Kim, A. R. Shenoy, P. Kumar, R. Das, S. Tiwari, J. D. M. Micking, A family of IFN-γ-inducible 65-kD GTPases protects against bacterial infection. *Science* **332**, 717–721 (2011).
41. A. R. Shenoy, D. A. Wellington, P. Kumar, H. Kassa, C. J. Booth, P. Cresswell, J. D. MacMicking, GBP5 promotes NLRP3 inflammasome assembly and immunity in mammals. *Science* **336**, 481–485 (2012).
42. H. S. Kaya-Okur, S. J. Wu, C. A. Codomo, E. S. Pledger, T. D. Bryson, J. G. Henikoff, K. Ahmad, S. Henikoff, CUT&Tag for efficient epigenomic profiling of small samples and single cells. *Nat. Commun.* **10**, 1930 (2019).
43. Y. Li, K. Nakka, T. Olender, P. Gingras-Gelinas, M. M. Wong, D. C. L. Robinson, H. Bandukwala, C. G. Palii, O. Neyret, M. Brand, A. Blais, F. J. Dilworth, Chromatin and transcription factor profiling in rare stem cell populations using CUT&Tag. *STAR Protoc.* **2**, 100751 (2021).
44. N. D. Heintzman, R. K. Stuart, G. Hon, Y. Fu, C. W. Ching, R. D. Hawkins, L. O. Barrera, S. Van Calcar, C. Qu, K. A. Ching, W. Wang, Z. Weng, R. D. Green, G. E. Crawford, B. Ren, Distinct and predictive chromatin signatures of transcriptional promoters and enhancers in the human genome. *Nat. Genet.* **39**, 311–318 (2007).
45. B. E. Bernstein, M. Kamal, K. Lindblad-Toh, S. Bekiranov, D. K. Bailey, D. J. Huebert, S. McMahon, E. K. Karlsson, E. J. Kulbokas III, T. R. Gingeras, S. L. Schreiber, E. S. Lander, Genomic maps and comparative analysis of histone modifications in human and mouse. *Cell* **120**, 169–181 (2005).
46. B. J. Frisch, J. M. Ashton, L. Xing, M. W. Becker, C. T. Jordan, L. M. Calvi, Functional inhibition of osteoblastic cells in an in vivo mouse model of myeloid leukemia. *Blood* **119**, 540–550 (2012).
47. B. Zhang, Y. W. Ho, Q. Huang, T. Maeda, A. Lin, S. U. Lee, A. Hair, T. L. Holyoake, C. Huettner, R. Bhatia, Altered microenvironmental regulation of leukemic and normal stem cells in chronic myelogenous leukemia. *Cancer Cell* **21**, 577–592 (2012).
48. S. F. Ziegler, F. Ramsdell, K. A. Hjerrild, R. J. Armitage, K. H. Grabstein, K. B. Hennen, T. Farrah, W. C. Fanslow, E. M. Shevach, M. R. Alderson, Molecular characterization of the early activation antigen CD69: A type II membrane glycoprotein related to a family of natural killer cell activation antigens. *Eur. J. Immunol.* **23**, 1643–1648 (1993).
49. M. López-Cabrera, A. G. Santis, E. Fernández-Ruiz, R. Blacher, F. Esch, P. Sánchez-Mateos, F. Sánchez-Madrid, Molecular cloning, expression, and chromosomal localization of the human earliest lymphocyte activation antigen AIM/CD69, a new member of the C-type animal lectin superfamily of signal-transmitting receptors. *J. Exp. Med.* **178**, 537–547 (1993).
50. L. X. Heinz, J. Lee, U. Kapoor, F. Kartnig, V. Sedlyarov, K. Papakostas, A. Cesar-Razquin, P. Essletzbichler, U. Goldmann, A. Stefanovic, J. W. Bigenzahn, S. Scorzoni, M. D. Pizzagalli, A. Bensimon, A. C. Muller, F. J. King, J. Li, E. Girardi, M. L. Mbow, C. E. Whitehurst, M. Rebsamen, G. Superti-Furga, TASL is the SLC15A4-associated adaptor for IRF5 activation by TLR7-9. *Nature* **581**, 316–322 (2020).
51. M. I. Davis, J. P. Hunt, S. Herrgard, P. Ciceri, L. M. Wodicka, G. Pallares, M. Hocker, D. K. Treiber, P. P. Zarrinkar, Comprehensive analysis of kinase inhibitor selectivity. *Nat. Biotechnol.* **29**, 1046–1051 (2011).
52. J. R. Burke, M. A. Pattoli, K. R. Gregor, P. J. Brassil, J. F. MacMaster, K. W. McIntyre, X. Yang, V. S. Iotzova, W. Clarke, J. Strnad, Y. Qiu, F. C. Zusi, BMS-345541 is a highly selective inhibitor of I kappa B kinase that binds at an allosteric site of the enzyme and blocks NF-kappa B-dependent transcription in mice. *J. Biol. Chem.* **278**, 1450–1456 (2003).
53. R. Waelchli, B. Bollbuck, C. Bruns, T. Buhl, J. Eder, R. Feifel, R. Hersperger, P. Janser, L. Revesz, H. G. Zerwes, A. Schlapbach, Design and preparation of 2-benzamido-pyrimidines as inhibitors of IKK. *Bioorg. Med. Chem. Lett.* **16**, 108–112 (2006).
54. T. L. Bailey, C. Elkan, Fitting a mixture model by expectation maximization to discover motifs in biopolymers. *Proc. Int. Conf. Intell. Syst. Mol. Biol.* **2**, 28–36 (1994).
55. O. Silvennoinen, J. N. Ihle, J. Schlessinger, D. E. Levy, Interferon-induced nuclear signalling by Jak protein tyrosine kinases. *Nature* **366**, 583–585 (1993).
56. K. Shuai, C. Schindler, V. R. Prezioso, J. E. Darnell Jr., Activation of transcription by IFN-gamma: Tyrosine phosphorylation of a 91-kD DNA binding protein. *Science* **258**, 1808–1812 (1992).
57. C. Schindler, K. Shuai, V. R. Prezioso, J. E. Darnell Jr., Interferon-dependent tyrosine phosphorylation of a latent cytoplasmic transcription factor. *Science* **257**, 809–813 (1992).
58. X. Y. Fu, C. Schindler, T. Improta, R. Aebersold, J. E. Darnell Jr., The proteins of ISGF-3, the interferon alpha-induced transcriptional activator, define a gene family involved in signal transduction. *Proc. Natl. Acad. Sci. U.S.A.* **89**, 7840–7843 (1992).
59. Y. Kanno, C. A. Kozak, C. Schindler, P. H. Driggers, D. L. Ennist, S. L. Gleason, J. E. Darnell Jr., K. Ozato, The genomic structure of the murine ICSBP gene reveals the presence of the gamma interferon-responsive element, to which an ISGF3 alpha subunit (or similar) molecule binds. *Mol. Cell. Biol.* **13**, 3951–3963 (1993).
60. R. Sen, D. Baltimore, Multiple nuclear factors interact with the immunoglobulin enhancer sequences. *Cell* **46**, 705–716 (1986).
61. C. E. Grant, T. L. Bailey, W. S. Noble, FIMO: Scanning for occurrences of a given motif. *Bioinformatics* **27**, 1017–1018 (2011).
62. N. K. Wilson, S. D. Foster, X. Wang, K. Knezevic, J. Schütte, P. Kaimakis, P. M. Chilarska, S. Kinston, W. H. Ouwehand, E. Dzierzak, J. E. Pimanda, M. F. T. R. de Bruijn, B. Göttgens, Combinatorial transcriptional control in blood stem/progenitor cells: Genome-wide analysis of ten major transcriptional regulators. *Cell Stem Cell* **7**, 532–544 (2010).
63. M. R. Tijssen, A. Cvejic, A. Joshi, R. L. Hannah, R. Ferreira, A. Forrai, D. C. Bellissimo, S. H. Oram, P. A. Smethurst, N. K. Wilson, X. Wang, K. Ottersbach, D. L. Stemple, A. R. Green, W. H. Ouwehand, B. Göttgens, Genome-wide analysis of simultaneous GATA1/2, RUNX1, FLI1, and SCL binding in megakaryocytes identifies hematopoietic regulators. *Dev. Cell* **20**, 597–609 (2011).
64. S. Subramanian, J. A. I. Thoms, Y. Huang, P. Cornejo-Páramo, F. C. Koch, S. Jacquelin, S. Shen, E. Song, S. Joshi, C. Brownlee, P. S. Woll, D. Chacon-Fajardo, D. Beck, D. J. Curtis, K. Yehson, V. Antonenas, T. O'Brien, A. Trickett, J. A. Powell, I. D. Lewis, S. M. Pitson, M. K. Gandhi, S. W. Lane, F. Vafaee, E. S. Wong, B. Göttgens, H. Alinejad-Rokny, J. W. H. Wong, J. E. Pimanda, Genome-wide transcription factor-binding maps reveal cell-specific changes in the regulatory architecture of human HSPCs. *Blood* **142**, 1448–1462 (2023).
65. A. C. Feng, B. J. Thomas, P. K. Purbey, F. M. de Melo, X. Liu, A. E. Daly, F. Sun, J. H. Lo, L. Cheng, M. F. Carey, P. O. Scumpia, S. T. Smale, The transcription factor NF-κB orchestrates nucleosome remodeling during the primary response to Toll-like receptor 4 signaling. *Immunity* **57**, 462–477.e9 (2024).
66. F. Y. Tsai, G. Keller, F. C. Kuo, M. Weiss, J. Chen, M. Rosenblatt, F. W. Alt, S. H. Orkin, An early haematopoietic defect in mice lacking the transcription factor GATA-2. *Nature* **371**, 221–226 (1994).
67. X. Gao, K. D. Johnson, Y. I. Chang, M. E. Boyer, C. N. Dewey, J. Zhang, E. H. Bresnick, Gata2 cis-element is required for hematopoietic stem cell generation in the mammalian embryo. *J. Exp. Med.* **210**, 2833–2842 (2013).
68. R. J. Wozniak, S. Keles, J. J. Lugus, K. H. Young, M. E. Boyer, T. M. Tran, K. Choi, E. H. Bresnick, Molecular hallmarks of endogenous chromatin complexes containing master regulators of hematopoiesis. *Mol. Cell. Biol.* **28**, 6681–6694 (2008).
69. A. P. Hsu, E. P. Sampaio, J. Khan, K. R. Calvo, J. E. Lemieux, S. Y. Patel, D. M. Frucht, D. C. Vinh, R. D. Auth, A. F. Freeman, K. N. Olivier, G. Uzel, C. S. Zerbe, C. Spalding, S. Pittaluga, M. Raffeld, D. B. Kuhns, L. Ding, M. L. Paulson, B. E. Marciano, J. C. Gea-Banacloche, J. S. Orange, J. Cuellar-Rodriguez, D. D. Hickstein, S. M. Holland, Mutations in GATA2 are associated with the autosomal dominant and sporadic monocytopenia and mycobacterial infection (MonoMAC) syndrome. *Blood* **118**, 2653–2655 (2011).
70. R. E. Dickinson, H. Griffin, V. Bigley, L. N. Reynard, R. Hussain, M. Haniffa, J. H. Lakey, T. Rahman, X. N. Wang, N. McGovern, S. Pagan, S. Cookson, D. McDonald, I. Chua, J. Wallis, A. Cant, M. Wright, B. Keavney, P. F. Chinnery, J. Loughlin, S. Hambleton, M. Santibanez-Koref, M. Collin, Exome sequencing identifies GATA-2 mutation as the cause of dendritic cell, monocyte, B and NK lymphoid deficiency. *Blood* **118**, 2656–2658 (2011).

71. C. N. Hahn, C.-E. Chong, C. L. Carmichael, E. J. Wilkins, P. J. Brautigan, X.-C. Li, M. Babic, M. Lin, A. Carmagnac, Y. K. Lee, C. H. Kok, L. Gagliardi, K. L. Friend, P. G. Ekert, C. M. Butcher, A. L. Brown, I. D. Lewis, L. B. To, A. E. Timms, J. Storek, S. Moore, M. Altree, R. Escher, P. G. Bardy, G. K. Suthers, R. J. D'Andrea, M. S. Horwitz, H. S. Scott, Heritable GATA2 mutations associated with familial myelodysplastic syndrome and acute myeloid leukemia. *Nat. Genet.* **43**, 1012–1017 (2011).
72. J. Kazenwadel, G. A. Secker, Y. J. Liu, J. A. Rosenfeld, R. S. Wildin, J. Cuellar-Rodriguez, A. P. Hsu, S. Dyack, C. V. Fernandez, C. E. Chong, M. Babic, P. G. Bardy, A. Shimamura, M. Y. Zhang, T. Walsh, S. M. Holland, D. D. Hickstein, M. S. Horwitz, C. N. Hahn, H. S. Scott, N. L. Harvey, Loss-of-function germline GATA2 mutations in patients with MDS/AML or MonoMAC syndrome and primary lymphedema reveal a key role for GATA2 in the lymphatic vasculature. *Blood* **119**, 1283–1291 (2012).
73. P. Ostergaard, M. A. Simpson, F. C. Connell, C. G. Steward, G. Brice, W. J. Woollard, D. Dafou, T. Kilo, S. Smithson, P. Lunt, V. A. Murday, S. Hodgson, R. Keenan, D. T. Pilz, I. Martinez-Corral, T. Makinen, P. S. Mortimer, S. Jeffery, R. C. Trembath, S. Mansour, Mutations in GATA2 cause primary lymphedema associated with a predisposition to acute myeloid leukemia (Emberger syndrome). *Nat. Genet.* **43**, 929–931 (2011).
74. D. C. Bellissimo, N. A. Speck, RUNX1 mutations in inherited and sporadic leukemia. *Front. Cell Dev. Biol.* **5**, 111 (2017).
75. C. C. Homan, S. L. King-Smith, D. M. Lawrence, P. Arts, J. Feng, J. Andrews, M. Armstrong, T. Ha, J. Dobbins, M. W. Drazer, K. Yu, C. Bodor, A. Cantor, M. Cazzola, E. Degelman, C. D. DiNardo, N. Duployez, R. Favier, S. Frohling, J. Fitzgibbon, J. M. Klco, A. Kramer, M. Kurokawa, J. Lee, L. Malcovati, N. V. Morgan, G. Natsoulis, C. Owen, K. P. Patel, C. Preudhomme, H. Raslova, H. Rienhoff, T. Ripperger, R. Schulte, K. Tawana, E. Velloso, B. Yan, P. Liu, L. A. Godley, A. W. Schreiber, C. N. Hahn, H. S. Scott, A. L. Brown, The RUNX1 database (RUNX1db): Establishment of an expert curated RUNX1 registry and genomics database as a public resource for familial platelet disorder with myeloid malignancy. *Haematologica* **106**, 3004–3007 (2021).
76. H. Huang, M. Yu, T. E. Akie, T. B. Moran, A. J. Woo, N. Tu, Z. Waldon, Y. Y. Lin, H. Steen, A. B. Cantor, Differentiation-dependent interactions between RUNX-1 and FLI-1 during megakaryocyte development. *Mol. Cell. Biol.* **29**, 4103–4115 (2009).
77. A. Rajagopalan, Y. Feng, M. B. Gayatri, E. A. Ranheim, T. Klungness, D. R. Matson, M. H. Lee, M. M. Jung, Y. Zhou, X. Gao, K. V. Nadiminti, D. T. Yang, V. L. Tran, E. Padron, S. Miyamoto, E. H. Bresnick, J. Zhang, A gain-of-function p53 mutant synergizes with oncogenic NRAS to promote acute myeloid leukemia in mice. *J. Clin. Invest.* **133**, e173116 (2023).
78. S. C. McIver, K. J. Hewitt, X. Gao, C. Mehta, J. Zhang, E. H. Bresnick, Dissecting regulatory mechanisms using mouse fetal liver-derived erythroid cells. *Methods Mol. Biol.* **1698**, 67–89 (2018).
79. H. Im, J. A. Grass, K. D. Johnson, S. I. Kim, M. E. Boyer, A. N. Imbalzano, J. J. Bieker, E. H. Bresnick, Chromatin domain activation via GATA-1 utilization of a small subset of dispersed GATA motifs within a broad chromosomal region. *Proc. Natl. Acad. Sci. U.S.A.* **102**, 17065–17070 (2005).
80. H. S. Kaya-Okur, D. H. Janssens, J. G. Henikoff, K. Ahmad, S. Henikoff, Efficient low-cost chromatin profiling with CUT&Tag. *Nat. Protoc.* **15**, 3264–3283 (2020).
81. T. Fujiwara, H. O'Geen, S. Keles, K. Blahnik, A. K. Linnemann, Y. A. Kang, K. Choi, P. J. Farnham, E. H. Bresnick, Discovering hematopoietic mechanisms through genome-wide analysis of GATA factor chromatin occupancy. *Mol. Cell* **36**, 667–681 (2009).
82. E. M. Moresco, D. LaVine, B. Beutler, Toll-like receptors. *Curr. Biol.* **21**, R488–R493 (2011).

Acknowledgments: We thank T. Olander for consultation on CUT&Tag methodology. We thank the Carbone Cancer Center Flow Lab for flow cytometry and cell sorting services and Cancer Informatics Shared Resource for bioinformatic analysis support. **Funding:** This work was supported by the National Institute of Health grant R01DK68634 (E.H.B.), U01CA257666 (E.H.B.), Carbone Cancer Center P30CA014520 (E.H.B.), T32 HL07899 (V.L.T.), and F31 DK138794-01A1 (V.L.T.). **Author contributions:** Conceptualization: V.L.T., K.D.J., and E.H.B. Methodology: V.L.T., P.L., K.R.K., K.D.J., A.A.S., and E.H.B. Investigation: V.L.T., P.L., K.R.K., K.D.J., A.A.S., Z.S.A., A.E.M., A.K., and E.H.B. Formal analysis: V.L.T. and E.H.B. Data curation: V.L.T. and E.H.B. Validation: V.L.T., A.K., and E.H.B. Visualization: V.L.T. and E.H.B. Resources: V.L.T., K.D.J., M.B., and E.H.B. Project administration: V.L.T. and E.H.B. Funding acquisition: V.L.T. and E.H.B. Supervision: M.B., K.D.J., and E.H.B. Writing—original draft: V.L.T. and E.H.B. Writing—review and editing: all authors. **Competing interests:** The authors declare that they have no competing interests. **Data and materials availability:** The RNA-seq and CUT&Tag data generated in this study were deposited in GEO under the accession numbers GSE279155 and GSE279156, respectively, with the GEO access token (GSE279155: sdmrcgoullszbmz; and GSE279156: qdyhaawebfenfyp). All data needed to evaluate the conclusions in the paper are present in the paper.

Submitted 15 December 2024
Accepted 3 April 2025
Published 28 May 2025
10.1126/sciadv.adv3169